# EFFECTS OF AROMATIC RING ($C_6$) FUNCTIONALIZATION ON ELECTRONIC- TRANSPORT PROPERTIES OF ARMCHAIR GRAPHENE NANORIBBONS

MELESE SINU W/MARIAM

A THESIS SUBMITTED TO

THE MATERIALS SCIENCE PROGRAM

PRESENTED IN PARTIAL FULFILMENT OF THE REQUIREMENTS FOR THE DEGREE OF MASTER OF SCIENCES IN MATERIALS SCIENCE

ADDIS ABABA UNIVERSITY

ADDIS ABABA, ETHIOPIA

March, 2013

**ADDIS ABABA UNIVERSITY**

**SCHOOL OF GRADUATE STUDIES**

This is to certify that the thesis prepared by Melese Sinu W/Mariam entitled: Effects of Aromatic Ring ($C_6$) Functionalization on Electronic-Transport Properties of Armchair Graphene Nanoribbons and submitted in partial fulfillment of the requirements for the Degree of Master of Science (Materials Science) complies with the regulations of the University and meets the accepted standards with respect to originality and quality.

Signed by the Examining Committee:

Advisor: Prof. Javed Mazher Signature _____ Date 08.03.2013

Examiner: Dr. Ahmed Mustefa Signature _____ Date _____

Chairman: Prof. Teketel Yohannes Signature _____ Date 11/03/2013

**Abstract**

Two dimensional structures like graphene nanostructures exhibit various physical properties on in-plane anchoring of functional groups. We have investigated the electronic band structure, the density of states (DOS), and the current-voltage (I-V) characteristics of pristine and armchair nanoribbons (AGNRs) functionalized with aromatic ring ($C_6$) by first- principles calculations with the help of ab-initio DFT code. A $C_6$ ring structure is in-plane anchored to the nano-ribbon to maximize the effects of functionalization on the properties of the nanostructures of various widths. Samples are theoretically modeled, both in the periodic and open system nano-device configurations, by using arm-chair nanoribbons of different widths with and without ring attachments. Subsequently, the as-prepared nano-devices are simulated and their I-V characteristics are studied. The results of these simulations are analysed by using the charge transfer, which takes place during the final self consistent calculation routines amongst the C-ring and its ribbons. We found a significant amount of change in the electronic density of states of the semiconducting ribbons due to the presence of $C_6$-rings. Also, we have demonstrated that the C-ring attachment can be effectively used to tailor the energy bandgaps of the semiconducting ribbons. In addition to this we have also showed the nano-device feasibility of such ring functionalized ribbons. The property of bandgap dependence on aromatic ring is also studied. Finally the prospects of functionalized nanostructures of graphene are also discussed in this thesis, especially, the electronic and transport properties of armchair ribbons are discussed with respect to ring functionalizations.

**Acknowledgements**

First of all I would like to thank the almighty God for giving me a chance to join the masters program and giving me health.

There are no enough words to express my deepest gratitude and profound thanks to my thesis advisor, Professor Javed Mazher for his guidance, co-operation, comments, and encouragement.

I would also like to acknowledge Professor Teketel Yohannes, Chair of Materials Science program, for his help in research methods and encouragement in my study.

Finally, I wish to express my warmest thanks to my brother, Professor Moges W/meskel

University of Georgia, USA, for supporting me during my two years stay here at Addis-Ababa University and to my family for their patience and support in every possible ways.

## Table of Contents

## List of Tables

## List of Figurers

# CHAPTER-ONE

## 1. Introduction

Recently, the functionalization of graphene nanostructures with the cyclic compounds has attracted lots of scientific interest [1]. Herein the functional groups are composed of at least one aromatic ring of C-atoms. It is to be noted that the functionalization of graphene nanostructures have found to intensively increase their graphene's industrial deployability by enhancing their physicochemical properties like solubility [2], mono dispersive nature, electron transmissions, tailoring the electronic band structure, etc. Generally, researchers used anchoring or attachment of nanostructures with various functional groups to impart the properties of these groups to the nanostructures by the process of electron transfer. The interaction of the parent nanostructures with functional group is usually found to affect the important opto-electric properties of nanostructures and the nano-structural charge carrier dynamics.

In this thesis we intend to study the outcome of anchoring a simple $C_6$, hexagonal ring to the graphene nano-ribbon (GNR) in the in plane geometry. Thus, it is expected that the $\pi$ electron of the $C_6$ ring would have maximum possible interaction with the $\pi$ electron of the ribbon edge structures. Graphene is a 2D single layer of carbon atoms with the hexagonal packed structure. The carbon bonds are $sp^2$ hybridized, where the in-plane $\sigma$ C-C bond is one of the strongest bonds in materials and the out-of-plane $\pi$ bond, which contributes to a delocalized network of electrons, which is responsible for the electron conduction of graphene and provides the weak interaction among graphene layers. By cutting the graphene into narrow stripes, we usually obtain Nanoribbons (GNRs) with one-dimensional carrier freedom. Depending on the termination style, we can divide them into two ribbon types, namely Armchair and Zigzag. Their results show that all armchair GNRs are semiconductors [3]. We are using armchair GNRs as a parent nanostructure for the very purpose of $C_6$ functionalization. In this thesis we have performed a theoretical study on the ribbons of varying widths (3,6,9, and 12 of C-rows) by using the ab-initio density functional theory (DFT) to determine the effect of aromatic ring ($C_6$) functionalization on the electronic-transport properties of AGNRs.

## 1.1 Graphene:

Graphene is a rapidly rising star on the horizon of materials science and condensed matter physics which was discovered in 2004 by Andre Geim et al [4]. Graphene is the name given to a flat monolayer of carbon atoms tightly packed into a two-dimensional (2D) honeycomb lattice, and is a basic building block for graphitic materials of all other dimensionalities as shown in the Figure 1.1 It can be wrapped up into 0-D fullerenes, rolled into 1-D nanotube or stacked into 3-D graphite [5, 6].

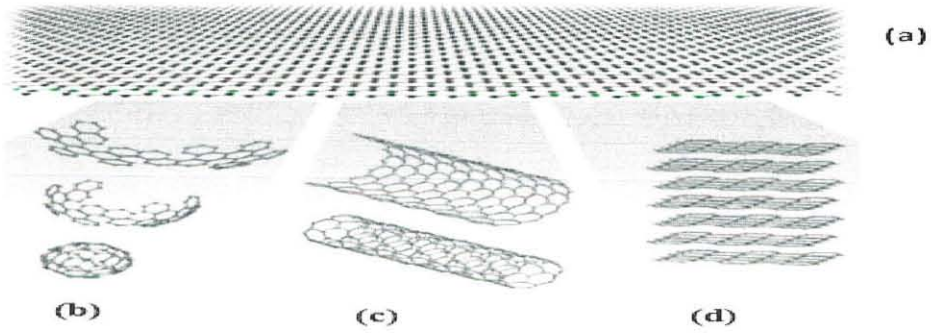


**Figure 1.1 Allotropes of Graphene, a 2D building material for carbon materials, for various dimensionalities; (a) Monolayer, (b) Graphene can be wrapped up into Bucky balls, (c) It can be rolled up into nanotubes and (d) stacked into bilayer or graphitic multilayers.**

## 1.2 Electronic Properties of Graphene

Graphene is the ideal bi-dimensional (2D) allotropic form of carbon where the atoms are periodically arranged in an infinite hexagonal network. Carbon has four valence orbitals (the $2s$, $2p_x$, $2p_y$ and $2p_z$ orbitals,) where $p_z$ is perpendicular to the sheet), the ($s$, $p_x$ , $p_y$ ) orbitals combine to form the in plane $\sigma$ (bonding or occupied) and $\sigma^*$ (anti-bonding or unoccupied) orbitals. The $\sigma$ bonds are strong covalent bonds responsible for most of the binding energy and for the elastic properties of the graphene sheet. The remaining $p_z$ orbital, pointing out of the graphene sheet cannot couple with the $\sigma$ states. The

interactions with neighboring $p_z$ orbitals creates the delocalized $\pi$ (bonding) and $\pi^*$ (anti-bonding) orbitals.

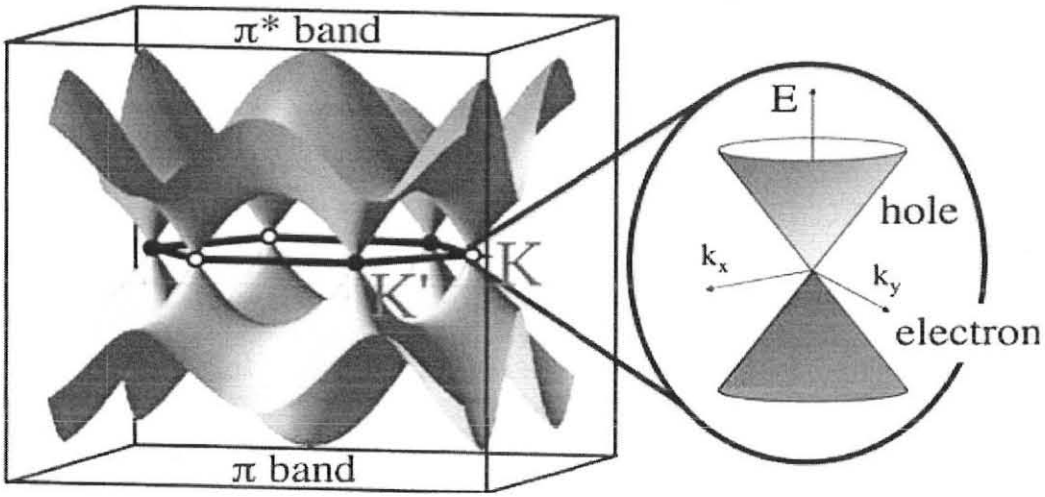


**Figure 1.2 Graphene's $\pi$ and $\pi^*$ electronic bands. The $\pi$ and $\pi^*$ bands are usually symmetric with respect to the valence and conduction bands. Linear dispersion relation close to the K and K' points of the first 2D Brillouin zone are illustrated by using the Dirac cone [6].**

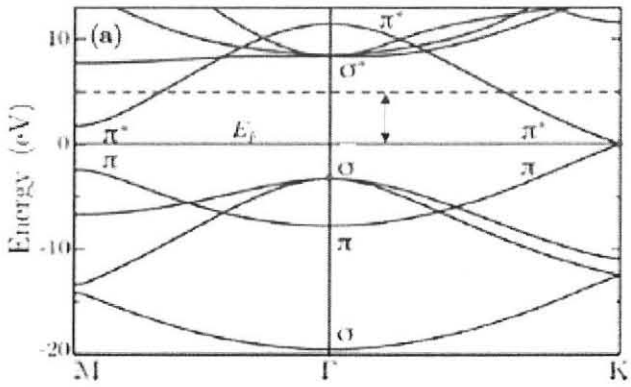


**Figure 1.3 Band structure of graphene.**

Since the bonding and anti-bonding $\sigma$ bands are well separated in energy (>12 eV at $\Gamma$ ), they are frequently neglected in semi-empirical calculations as they are too far away from the Fermi level to play a role as depicted in the Figure1.3. Only the remaining two $\pi$

bands are thus needed to describe the electronic properties of graphene. Indeed, the bonding $\pi$- and anti-bonding carbon $\pi^*$-orbitals do form the wide electronic valence and conduction bands which cross the Fermi level at high-symmetry points in the Brillouin zone of graphene. The $\pi$ and $\pi^*$ bands are quasi-linear (linear very close to K or K' and near the Fermi energy). Graphene is thus highly specific for this linear energy momentum relation, leading to mass less fermions. The linear $\pi$ and $\pi^*$ bands for the Dirac fermions becomes as, $E = hV_f K$. Where $V_f = 10^6$m/s which is the Fermi velocity. In graphene, charge carriers mimic relativistic particles with zero mass.

### 1.3 General Properties of Graphene

Graphene is an amazingly pure substance due to its simple, orderly structure based on tight, regular, and atomic bonding. Carbon is a nonmetal, so we might expect graphene to be one too. In fact, it behaves much more like a metal (though the way it conducts electricity is very different), and that amuses some scientists to describe it as a semimetal or a semiconductor [7].

#### i) Strength and Stiffness

Graphene is super strong even stronger than diamond!. Graphene is believed to be the strongest material yet discovered, some 200 times stronger than steel. Remarkably, it's both stiff and elastic (like rubber), so we can stretch it by an amazing amount (20 - 25 percent of its original length) without breaking it. That's because the flat planes of carbon atoms in graphene can flex relatively easily without breaking the atoms apart [7]. Graphene has the highest strength (130 GPa) [9].

#### ii) Thinness and Lightness

As graphene is only one atom thick is bound to be pretty light [7]. A sheet of graphene is thinnest material in the universe, just a single layer of C-atoms which are locked together in a strongly bonded honeycomb pattern. This makes graphene the thinnest material. One

needs to stack 3 million graphene sheets on top of each other to get a pile of one millimeter high.

**iii) Electrical and Thermal Conductivity**

Materials that conduct heat very well also conduct electricity well, because both processes transport energy using electrons. The flat, hexagonal lattice of graphene offers relatively little resistance to electrons, carrying the electricity even better than copper. Graphene has thermal conductivity of (3000 W/mK) [9]. The electrons in graphene have a longer mean-free path than they have in any other material [7].

**iv) Optical Properties**

As a general rule, the thinner something is, the more likely it is to be transparent. Photons are more likely to penetrate through thin objects than thick ones. Super-thin graphene, being only one atom thick, is almost completely transparent and transmits about 97 – 98 percent of light (compared to about 80 – 90 percent for a basic, single pane of window glass) [7]. The measured white light absorbance of suspended single layer graphene is 2.3% with a negligible reflectance (0.1%), and this absorbance increases linearly with the layer numbers [ 8-9 ].

**v) Impermeability**

Sheets of graphene have such closely knit carbon atoms that they can work like super-fine atomic nets, stopping other materials from getting through. That means graphene is useful for trapping and detecting gases [7].

**1.4 Graphene Nanoribbons (GNRs)**

Although graphene has drawn tremendous attention for studies of its fundamental structural and electronic properties in recent years, the absence of an energy gap in graphene poses a challenge for conventional semiconductor field-effect transistor (FET) device operations. Previous studies have shown that an energy gap can be opened up by

patterning graphene into ribbons ~10 nm in width. When graphene is patterned along one specific direction, a novel quasi one-dimensional (1D) structure is obtained, which is a strip of graphene, referred as graphene nanoribbons (GNR) [12].

### 1.5 Geometric Structures of GNRs

The typical width of GNR is of nanometers. GNRs are a one dimension (1D) structure with confinement of carriers in two directions [12,13]. Depending on the termination style, GNR can be divided into two kinds: Armchair and Zigzag (Figure. 1.4 shows the structures of Armchair and Zigzag GNRs). Adopting the standard convention, the width of armchair GNRs is classified by the number of dimer lines ($N_a$) across the ribbons. Likewise, the one of zigzag GNRs is classified by the number of zigzag chains ($N_z$) across the ribbons [14]. The width of an armchair ribbon ($W_{ac}$) can be defined in terms of the number of dimer lines $N_a$, as $W_{ac} = (N_a - 1)\frac{\sqrt{3}}{2}a$, with a = 1.42 Å the nearest neighbor distance. The width of a zigzag ribbon ($W_{zz}$) is identified with the number of zigzag chains Nz, as $W_{zz} = (N_z - 1)\frac{3}{2}a$, with a = 1.42 Å as the nearest neighbor distance.

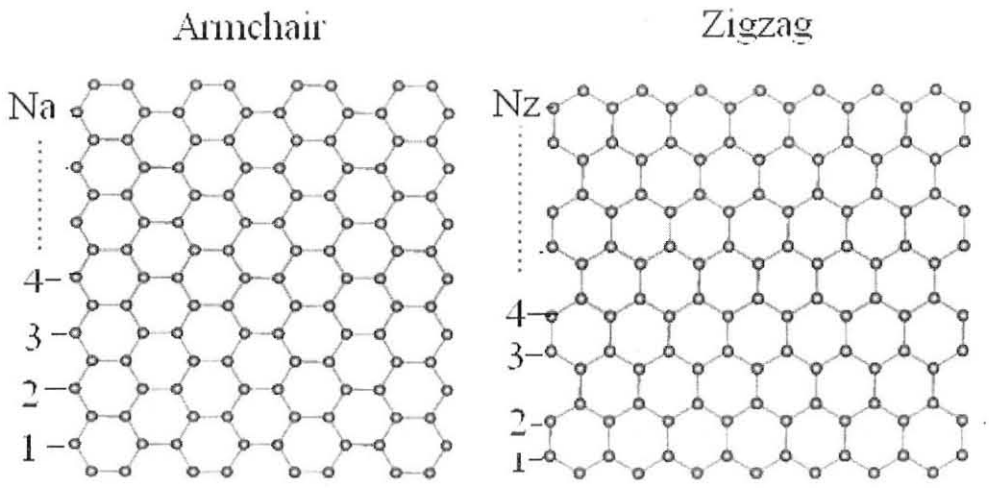


**Figure 1.4 Structure of armchair and zigzag nanoribbons [14]**

### 1.6 Electronic Properties of Armchair GNRs

Electronic structure of the armchair GNRs is very rich in energy band features due to the fact that it is neither insulating nor metallic; its energy gap at the zone center of the first brillouin zone varies from the metallic to semiconducting depending upon the ribbons widths. As shown in the Figure 1.4, among the armchair GNRs, the ribbon width is defined by the number of dimer lines ($N_a$) across the ribbons. Their electronic structures have been carefully investigated by DFT calculations. Their results show that all armchair GNRs are semiconductors with energy gaps, which decrease as a function of increasing ribbon widths. As seen from Figure 1.5 the energy gaps of ribbon is a function of its width. The gaps are well separated into three categories depending on the integral dependency of the width which is given by: $N_a$ = 3p, 3p + 1, 3p + 2 (p is integer). Moreover, the gap size hierarchy is also found to be well separated. $N_a$ = 3p + 1 categories has the largest energy gap, while the $N_a$ = 3p + 2 series is the smallest one.

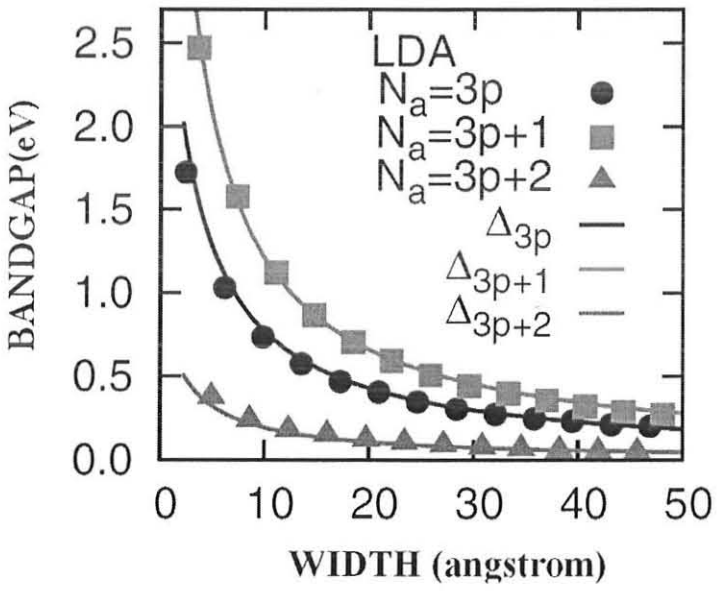


**Figure 1.5 The variation of band gaps of armchair GNRs with DFT calculations [12].**

Although, the armchair GNRs have three typical families (corresponding to $N_a$ = 3p, 3p + 1, 3p + 2, respectively) with distinguished energy gaps, they have similar band shapes as

shown in the Figure 1.5, which describes the dependency of a band gap originating from quantum confinement. Thus, the bandgap oscillations in between 4.1 eV to 4.8 eV can be predicted for semiconducting armchair ribbons as a function of their width of 5-16 C atom rows [10, 11]. These oscillations introduce the possibility of tailoring their electronic structure. It should be noted that the physical properties of 3p type of armchairs lies in between the 3p+1 and 3p+2 types of ribbons, which is also clear from the Figure 1.5, thus 3p is the widely used system for the study of arm chair ribbons. The reported values of the intermediate bandgap oscillations for the 3p ribbons as a function of the width of the system can be related to their intermediate values of density of electrons and the nature of electron delocalization [10]. Some recent reports from Fei Ma et. al. (2012) also shows the oscillatory trends in the AGNR bandgaps with ribbons having the widths of 4 to 16 C-atom rows. However, the ribbons of Ma et al are H passivated and the reported bandgap values are oscillates from 1.8 eV to 0.4 eV.

## 1.7 Functionalization of Graphene

Modification of GNRs with various types of elements and functional groups can give us a variety of properties, such as semiconducting with a wide range of band gap, metallic, ferromagnetic, anti-ferromagnetic, half-metallic, half-semiconducting. It was demonstrated by theoretical calculations that different functional groups at the edge of nanoribbons can significantly affect their electronic structure close to Fermi level [15]. The functionalization of graphene is found to modify its electronic structure; it can be achieved from either nano ribbon edge modification by anchoring the edge with functional groups or by substitution and absorption of the foreign groups inside the graphene monolayer [15]. $Fe_n$ and $Ti_n$ have found to induced half metallic character to arm-chair ribbons [16]. It should be noted that the chemical functioanlization of graphene with the use of cyclic carbon rings is a novel route to induce useful properties in the inherently hydrophobic and semi-metallic graphene. It has been reported that the cyclic benzene type compounds like aryne can induce hydrophilic nature in the graphene rendering its ready for industrial manufacturing or common aqueous synthesis. But for the pure graphene sheet the chemical functionalization via adsorption of cycling rings is

found to be very weak; the adsorption energy value of the $C_6$ ring with the graphene is just -0.204 eV [20]. Hence, a novel method has been explored to functionalized the graphene by using its nanaostructures. The value of adsorption energy is found to be significantly enhanced if we attach the aryne like cyclic groups at the armchair edges of the ribbon; a attachment energy of -5.864 eV has been obtained [20]. But unfortunately the authors in the ref [20]. did not perform any study related with the effects of the ribbon widths on such functionalization. Neither had they done any electron transport or electron density of states study on such $C_6$ functionalized study. However, the it is clear from the ref [20] that edges of the armchairs GNRs is a feasible way to induce functionalization in the graphene. Thus, we found that it is necessary to perform a generic study using a $C_6$ ring on the edges of graphene ribbons of various widths to systematically analyze the effects of functionalization on electro-transport properties of graphene. It is to be noted that the ring that we have taken is a part of graphene itself.

### 1.7.1 Covalent Functionalization of Graphene

Graphene sheet can be covalently functionalized. Such covalent functionalization enables to dissolve large quantities of graphene nanostructures in the industrial solvents [18]. Thus, covalent functionalization facilitates the industrial manufacturing of functional nanocomposites of graphene. Molecules such as sugars are reported to be functionalized with graphene in various concentrations . Theoretical studies on the $C_6$ absorption on armchair graphene nano-ribbons shows high degree of structural stabilities after the functionalization. Chemical functionalization with aryne groups leads to changes in the electronic bandgap of graphene, which is dependent on the coverage of the adsorbed cyclic groups [20]. It is found that the bandgap in fact oscillates on increasing the number of the functional groups. The two, four and six $C_6$ groups adsorption on the edges of the graphene yield the energy bandgap variations of 0.327, 0.925 and 0.190 eV.

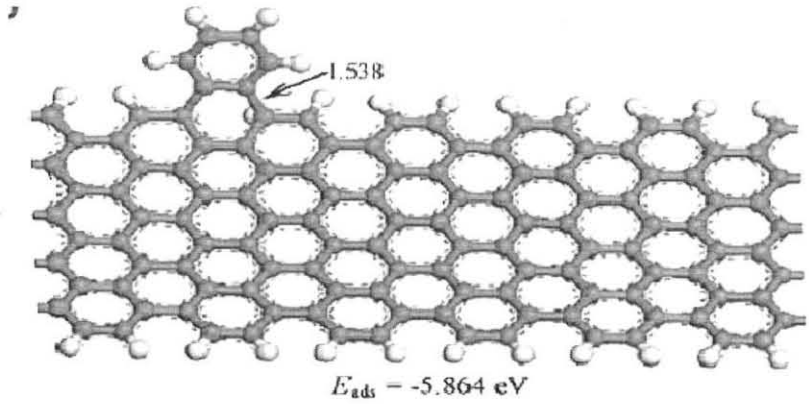


**Figure 1.6 Chemical functionalization of an individual $C_6$ ring adsorbed on the top edges of the armchair graphene nanoribbon (3p+1). It is clear that the functional group is perfectly resting on the seat-site of the arm chair edge [20].**

However, the adsorption of $C_6H_4$ groups on armchair graphene nanoribbon renders its bandgap be increased by 0.027 eV (for one $C_6H_4$ group) and 0.190 eV (for two $C_6H_4$ group), respectively [20]. It is found that graphene nanoribbon has much higher reactivity toward $C_6H_4$ groups. The most important is that the band structures of graphene systems near the Fermi level are greatly disturbed after covalent functionalization of $C_6H_4$ groups. This leads to an opening of band gaps of graphene nano-ribbons to different degrees. Hence the graphene nano-ribbons can be effectively functionalized with cyclic benzene like aryne groups at a high degree with large stabilities. [20]. The simulational studies also show that the bandgap for 3AGNR, which is 0.44eV for the case of pristine form, can be increased to 0.69eV for the same ribbon (3p type) with single $C_6$ ring attached.

Aromatic functionalization of graphene is also theoretically studied before by using ab-initio DFT NEGF methods [18]. The aromatic anthracene molecule -- having three $C_6$ like rings – is functionalized at the edges of the armchair graphene ribbon and the electro-transport properties of the graphene have been investigated. In this study it has been revealed that the organic molecule adsorption enhances the current transport characteristics of the '3p +2' type AGNRs in a two-probe configuration [21]. However,

the adsorptions of the linear polyaromatic hydrocarbons of anthracene on the ribbon decrease the band structure energy, which is the stability parameter in this study. The energy decreases from the initial value of the -1548.21 eV for the bare AGNRs to -1946.59 eV for the doped systems [21]. The variations in the device stability with the chemical functionalization also establish the fact that these systems could be useful to simulate the effects on the electronic transport of AGNRs, for development of graphene based sensor devices. Many recent research reports are also devoted towards the study of polycyclic aromatic hydrocarbon consisting of three fused benzene rings for the scintillator detectors performances of high energy photons, electrons and alpha particles; the I-V measurements of such ring functionalized devices changes on the absorptions of highly energetic particles [21]. Hence its very useful to simulate the electronic-transport performances of the system properties of bare AGNR and AGNR with attached bio-objects. At the same time the study of the ring functionalization is also useful for the graphene based glucose sensors [19]. It is found that due to the transfer of the charges from the bio-objects to the graphene, the electro-transport properties of graphene enhances. For instance, Chowdhury et al (2011) found that the calculated charge of bare AGNR is about 175.96q (where q is the electronic charge) compared to a charge of 219.94q in the case of AGNR with attached bio-objects [21]. It is interesting to note that the results for the interaction between hydrocarbons and semiconducting ribbons demonstrate a clear increase in the conductance of semiconducting ribbons, whereas, for the case of ZGNRs – metallic in nature—such physical features are completely absent. The simulation results for (3p+1) AGNRs indicate that the conductivity of the ring ($C_6$) attached ribbon increases due to charge transfer from the ring to the ribbon [20].

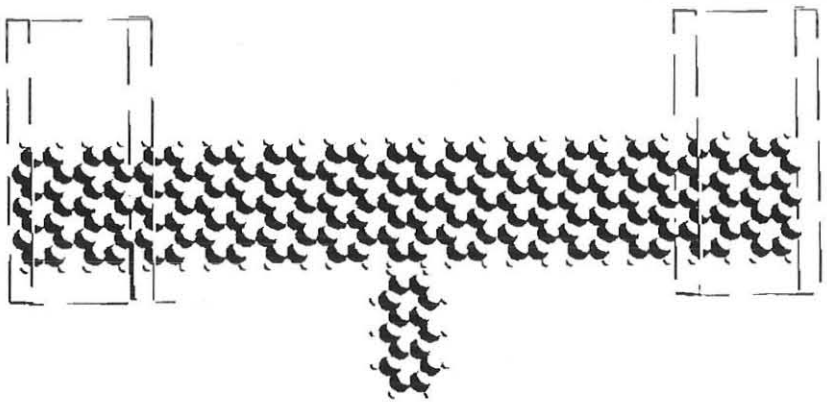

**Figure 1.7 Schematic configuration of a two-probe system for an armchair nanoribbon of ten unit cells in length with attached anthracene molecule [21].**

### 1.7.2 Non-Covalent Functionalization of Graphene

The non-covalent interactions are based on Vander Waals forces or π-π stacking of aromatic molecules on the graphene plane. The advantage is that this does not disrupt the extended π-conjugation on the graphene surface, unlike covalent functionalization [17]. But there is a great possibility to tailor the charge carrier density and density of states by this type of functionalization, whose effect is similar to that of application of local or gate related electric field. Graphene can be functionalized through non-covalent modification without affecting its structure by wrapping it with surfactants or through π-π interaction with aromatic molecules such as 1-pyrenebutanoic acid succinimidyl ester (PyBS) (I) [22]. Thus by this type of functionalization, we cannot tune the bandgap or density of states in the graphene. In this thesis we are intended to study the covalent type of functionalization of AGNRs by using the $C_6$ ring, so that, we can tailor the electronic structure of graphene nanostructures as much as possible.

### 1.7.3 Pure $C_6$ Ring functionalization of Graphene Nano ribbons (GNRs)

For the first time we are studying the effect of attachment of the just a carbon- ring on the armchair graphene nanoribbons of various 3p type widths. It is to be noted that the pure ac-GNRs have semiconducting nature and the electronic states are also few and with the increase in the width of the ribbons the DOS increases. It would be interesting to see the effects ring on the ac-GNR's nature and density of states with the covalent and periodic ring attachments and in respect to the variation in ribbon-widths. This is one of the prime objectives of the thesis. As a consequence of the attachment of aromatic ring ($C_6$) to the edge of the AGNRs, which also resembles for the semi-conductivity of the ribbon, it is expected that the aromatic ring either accepts the electrons of the ribbon or donates its charges to the ribbons. In both cases, the electronic properties of the ribbon tailored depend on the amount of charge transferred amongst the functional groups and the parent ribbons. Therefore, AGNRs are the most obvious choice, because of their semi-conductivity; they can be used in organic switches and sensors. A slight change in their electronic density of state due to functional group ($C_6$) attachment can induce large change in their electrode conductivity. In summary, it has been reported earlier that the aromatic compounds like aryne, anthracene, pyridine, aniline, etc, when functionalized with AGNRs induces different types of changes in ribbons [19, 20, 21]. Nevertheless, to the best of our knowledge, a generic electronic-transport study of the effect of just an aromatic ring has never been performed before, which is a major motivational factor for this thesis.

(a)

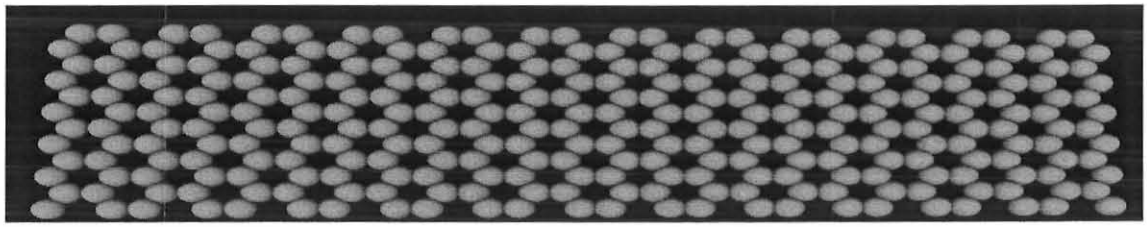

(b)

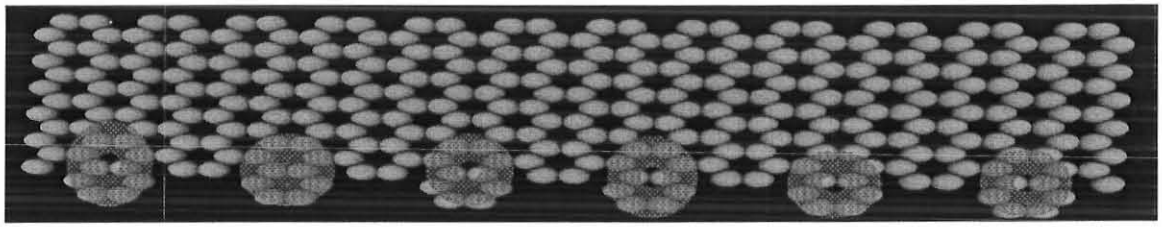

**Figure 1.8 Armchair graphene nano-ribbon's functionalized through C-ring (a) pristine ac-GNR without and ring attachment (b) one of the side armchair edges ribbon is attached by c-rings in a periodic fashion.**

# CHAPTER TWO

## 2. Objectives

### 2.1 General Objectives

- To study the graphene armchair nanostructures and the effect of aromatic $C_6$ ring functionalization on its electronic - transport properties.

### 2.2 Specific Objectives

- To model the armchair graphene nano-ribbon structures.
- To model the aromatic ring functionalization of armchair graphene nano-ribbon.
- To investigate the electronic transport properties of functionalized armchair graphene nanoribbons.
- To simulate the I-V measurements on graphene armchair nanoribbons in the functionalized and unfunctionalized state.

## CHAPTER THREE

### 3. Methodology and Simulation

The physical, chemical and electronic properties of a matter, responsible for its potential applications, are usually described by its electronic structure. So, the study of electronic structure of a matter has been a central issue of research amongst the scientists. In due course of time, new theoretical methods like ab-initio or first principle, Semi-empirical, Density Functional Theory has been developed for the systematic study of electronic structure. A number of methods amongst the semi-empirical to ab-initio (QM) approaches have been developed for approximating the solution for many electron systems. The former schemes usually need some parameters that are taken from or adjusted to experiments [23]. Thus, the quantum mechanical methods are based on solving the time-independent Schrödinger equation for electrons of a molecular system as a function of the nuclei positions. Although semi-empirical calculations are much faster than their ab-initio counterparts, if some parameters for semi-empirical simulations are not available, or some phenomena of a system are not yet known, one must rely only on ab-initio calculations [23].

The Hamiltonian ($\hat{H}$) for a molecular system comprising N nuclei and n electrons is given by:

$$\hat{H} = -\frac{h^2}{2}\sum_{I=1}^{N}\frac{1}{M_I}\nabla_I^2 - \frac{h^2}{2m}\sum_{i=1}^{n}\nabla_i^2 - \sum_{I=1}^{N}\sum_{i=1}^{n}\frac{Ze^2}{r_{i,I}} + \sum_{I=1}^{N}\sum_{J=1}^{N''}\left[\frac{Z_I Z_J e^2}{r_{I,J}}\right] + \sum_{i=1}^{n}\sum_{j=1}^{n'}\left[\frac{e^2}{r_i, j}\right] \quad \ldots (1)$$

### 3.1 Ab-initio Methods or First Principle Techniques

Ab-initio is the Latin term for "from first principles", or, "from scratch". We begin with fundamental physical properties, and we calculate how electrons and nuclei interact .Most often this requires solving approximations to the time independent Schrödinger equation. The advantage of ab-initio methods is the accuracy with which calculations are

performed. It is quite useful for a broad range of systems and does not depend on the experimental data. However, these methods can be successfully applied to small systems and are computationally expensive forms. These methods are more suitable for small systems with tens of atoms, for the systems without experimental data or for the systems that require high accuracy. It must be noted that ab-initio is the accurate and precise of all of the currently available in molecular modeling.

### 3.2 Born-Oppenheimer Approximation (BO)

On the way towards the ab-initio DFT description of a solid, the first approximation is to treat electron and nucleon motions independently, exploiting the fact that their motions take place in different time scales. In simple words, the electrons move a lot faster than the heavy nuclei. Consequently, it is a reasonable approximation to treat the nuclei as stationary within the electrons' reference system. The electron problem can be treated independently from the motion of the nuclei. This approximation was first proposed in 1927 by Born and Oppenheimer [24].

### 3.3 Density Functional Theory (DFT)

Density-functional theory in its earliest formulation by Hohenberg, Kohn and Sham aim at a description of the ground state properties of many-electron systems in terms of the electron density. DFT is based on the electron density and commonly used to calculate the electronic structure of complex systems containing many atoms such as large molecules or solids. In particular, ab-initio methods are nowadays indispensable for a thorough understanding of properties and to understand the physics of molecular systems or materials at the atomic scale. Among these, Kohn-Sham density functional theory (DFT) in the local density approximation (LDA) has been the main tool used by theoreticians for modeling the structural and electronic properties of molecules. The

basic idea of DFT is to replace the interacting many-electron problem with an effective single-particle problem. On the other hand, Hohenberg-kohn DFT underestimates the bandgaps of semiconductors and insulators by some tens of percent due to the simplified treatment of electron-electron correlations [23, 25, 26]. It has been known for some time that including some exact Hartree-Fock (HF) exchange in the modern hybrid density functional (B3LYP, PBE0, HSE, etc.) leads to substantially improved band gaps [27].

### 3.4 Hohenberg-Kohn Theorem and Equations

For many-electron system, the Hamilton operator $\hat{H}$ is given by a sum of the kinetic energy and the electron-electron, electron-nuclear and nuclear-nuclear interaction terms. Under the assumption that the nuclei are fixed and the many-electron Schrödinger equation for N electrons is given by

$$\hat{H}\Psi = \left[ -\frac{\hbar^2}{2m} \sum_{i}^{N} \nabla_i^2 + \sum_{i<j}^{N} \sum U(r_i - r_j) + \sum_{i}^{N} v_{ext}(r_i) \right] \Psi = E\Psi \qquad \ldots\ldots\ldots\ldots (2)$$

where $U(r_i - r_j) = e^2|r - r'|^{-1}$ is the electron-electron interaction and $v_{ext}(r)$ the external potential, which contains the static potential arising from the interaction of the electrons with the nuclei and a constant term arising from the nuclear-nuclear interaction. The formal solution of the many-electron Schrödinger Equation(1), defines a mapping from the external potential to the many-electron wave functions and thus also a mapping from external potential to the ground state wave function ,$\Psi_0$, and to the ground-state density, $n_0(r)$. The first part of the Hohenberg-Kohn theorem states that the mapping can be inverted so that the external potential is uniquely determined by the ground-state density except for a trivial additive constant shift of the external potential. Because of the mapping from the ground-state density to the external potential and of the mapping from the external potential to the many-electron wave functions, there is also a mapping from the ground-state density to the many-electron wave functions and to every expectation

value $\langle \Psi | \hat{O} | \Psi \rangle$, which means that every quantum mechanical observable is uniquely determined as a functional of the ground-state density. The second part of the Hohenberg-Kohn theorem states that the total energy functional E[n(r)] is minimal, if n(r) is the ground-state density $n_0(r)$, and that the minimum $E_0 = E[n_0(r)]$ is the ground-state energy.

### 3.5 Kohn-Sham Equations

The theory discussed above has transformed the problem of finding the minimum of $\langle \Psi | \hat{H} | \Psi \rangle$ for many-electron trial wave functions, $\Psi$, into the seemingly much more simple problem of finding the minimum of E[n(r)] for trial densities n(r). Here, the idea of Kohn and Sham, the introduction of a fictitious auxiliary non-interacting electron system with the same ground-state density is of extraordinary importance. Because the Hohenberg-Kohn theorem is valid for all interaction strengths (that is for all values of $e^2$), it is also valid for the choice $e^2 = 0$ which according to equation (2) describes a non-interacting system with U(r, r') = 0. By the Hohenberg- Kohn theorem the ground-state density uniquely determines the external potential in the non-interacting system. This potential is usually called the effective potential $v_{eff}$ (r). For the non-interacting system the total energy functional can be written as

$$E[n(r)] = T_s[n(r)] + \int n(r) v_{eff}(r) dr ,$$

Where, $T_s[n(r)]$ is the kinetic energy functional of non-interacting electrons.

### 3.6 Local Density Approximation (LDA)

The simplest approximation is to assume that the density can be treated locally as a uniform electron gas; the exchange correlation energy at each point in the system is the same as that of a uniform electron gas of the same density. This approximation was originally introduced by Kohn and Sham and holds for a slowly varying density. Using this approximation the exchange-correlation energy for a density $\rho(r)$ is given by

$$E_{xc}^{LDA} = \int \rho(r)\varepsilon_{xc}(\rho)dr \qquad \ldots\ldots\ldots\ldots \quad (3)$$

Where $\varepsilon_{xc}(\rho)$ is the exchange-correlation energy per particle of a uniform electron gas of density $\rho$ . The exchange-correlation potential is then given by

$$\upsilon_{xc}^{LDA}[\rho(r)] = \frac{\delta E_{xc}^{LDA}}{\delta \rho(r)} = \varepsilon_{xc}(\rho) + \rho(r)\frac{\partial \varepsilon_{xc}(\rho)}{\partial \rho} \qquad \ldots\ldots \quad (4)$$

For practical use of the LDA in calculations it is necessary to determine the exchange-correlation energy for a uniform electron gas of a given density. It is common to split $\varepsilon_{xc}(\rho)$ into exchange and correlation potentials $\varepsilon_{xc}(\rho) = \varepsilon_x(\rho) + \varepsilon_c(\rho)$. The exchange potential is given by

$$\varepsilon_{xc}[\rho(r)] = \frac{-3}{4}\left(\frac{3}{\pi}\right)^{\frac{1}{3}}\rho(r) \qquad \ldots\ldots\ldots (5)$$

Accurate values for $\varepsilon_c(\rho)$ have been determined from Quantum Monte Carlo (QMC) calculations.

### 3. 7 Non-Equilibrium Green's Function (NEGF)

Non-equilibrium Green's function (NEGF) is a general method for modeling non-equilibrium quantum transport in open mesoscopic systems with many body scattering effects. The transport properties such as current and transmission in two-probe devices can be calculated by using the Landauer Formalism which is mainly derived from the non-equilibrium green's function and is expressed as:

$$I = \frac{4e^2}{h}\int T(E)\left[F_L(E) - F_R(E)\right]dE \qquad \ldots\ldots\ldots\ldots \quad (6)$$

$T(E)$ is the transmission probability, $F_L(E)$ and $F_R(E)$ are the Fermi-function in left and right electrodes respectively.

## 3.8 Methodologies for Atomistic Simulation

### 3.8.1 SIESTA Software Package

**SIESTA** (Spanish Initiative for Electronic Simulations with Thousands of Atoms) is a computer program implementation, to perform efficient electronic structure calculations and ab-initio molecular dynamics simulations of molecules and solids. SIESTA's efficiency stems from the use of basis sets and from the implementation of linear-scaling algorithms which can be applied to suitable systems. A very important feature of the code is that its accuracy and cost can be tuned in a wide range, from quick exploratory calculations to highly accurate simulations matching the quality of other approaches, such as plane-wave and all-electron methods. The possibility of treating large systems with some first-principles electronic-structure methods has opened up new opportunities in many disciplines. The SIESTA program is distributed freely to academics and has become quite popular, being increasingly used by researchers in geosciences, biology, and engineering (apart from those in its natural habitat of materials physics and chemistry).

#### 3.8.1.1 Atomistix Toolkit (ATK)

It is a trans-SIESTA based software tool with a scripting language that provides with methods for first-principles electronic structure and transport calculations. ATK has a Python (a general purpose, high level programming scripting language) based interface called as Nano-Language along with a separate text file interface that is known as script generator. Atomistix ToolKit (ATK) offers unique capabilities for simulating electrical transport properties of nano-devices on the atomic scale. Based on an open architecture which integrates a powerful scripting language with a graphical user interface, ATK is a comprehensive platform for studies in nano-electronics, using both accurate first

principles Atomistix ToolKit (ATK) is the state-of –the-art DFT engine for electronic structure and transport calculations.

The unique feature of ATK to calculate ballistic tunneling current in nanostructures enables users to:

- Calculate the conductance of graphene nanoribbons of various edge types and shapes.
- Compute the current voltage characteristics when a finite bias is applied to the system.
- Study spins transport properties.
- Simulate the influence of a gate.
- Compute transistor characteristics.
- Investigate the details of the transport mechanisms.

The methods used in the software products are based primarily on Density Functional Theory (DFT) and Non-Equilibrium Green's Function (NEGF) techniques [28].

#### 3.8.1.2 Virtual Nano-Lab (VNL)

Virtual NanoLab (VNL) gives you access to a powerful set of modeling tools for investigating nanoscale structures through a user friendly graphical interface. The VNL software uses advanced software architecture and numerical methods to find solutions of the fundamental quantum mechanical equations describing the electronic properties of nanoscale objects, such as molecules, bulk and two-probe systems by use of the density functional theory (DFT) and non-equilibrium Green's functions (NEGF). Based on the these techniques, VNL can simulate the detailed electronic structure and transport properties of molecules, crystals, nanotubes, and two-probe devices. Virtual Nano-Lab (VNL) offers a rich set of powerful tools for investigating and analyzing the properties of nano-stuctures by simulating measurements through numerical calculations. It provides researchers and scientists convenient programs to design and build several types of

nanostructures, setup scripts for performing calculations and inspect, analyze, and visualize results.

Thus, Virtual Nano-Lab(VNL) is:

- ✓ Interactive builder for
  - ➢ Molecules
  - ➢ Crystals
  - ➢ Nanotubes
  - ➢ Two probe systems
- ✓ Interactive generation and export of Nano-Language scripts
  - ➢ Structure and geometries
  - ➢ Calculation and analysis
- ✓ Internal Nano-Language interpreter
  - ➢ Import user-defined geometry scripts for visualization or calculation setups.
- ✓ Local execution of Nano-Language scripts via drag-and drop.

The way we work with VNL is in many aspects similar to what we would do in an actual experiment [29].

#### 3.8.1.2.1 Steps in Working with VNL

- ➢ First we set up our system using either of the Molecular Builder, the Crystal Cupboard, or the Atomic Manipulator tools.
- ➢ After setting up our system, we specify the details of the DFT method that should be applied to our system. We do this using either the Method Editor or the NanoLanguage Scripter tool.
- ➢ Once the DFT method has been defined, we select the physical properties that should be extracted from the calculation. We do this by using the NanoLanguage Scripter tool.

- The calculation is then performed by submitting the job to the Job Manager tool or executing it from the command line.
- Finally, we analyze and inspect the obtained data by using the Nanoscope and the Result Browser tools.

The NanoLanguage scripts that are generated with VNL are performed with the Atomistix ToolKit (ATK) calculation engine. Since VNL is designed with ease-of-use in mind, someone should not have to be an expert in quantum chemistry and electronic structure calculations to use it. Instead, someone needs to focus on the physical properties of the systems under investigation, and let the program handle the details of the numerical models. The numerical methods used in VNL are primarily based on first principles (ab-initio) and do not, in principle, require any input parameters regarding the quantum-mechanical description of the atomic systems. Nevertheless, as is the case in most numerical simulations, a number of accuracy parameters must be specified to define the DFT and NEGF methods.

#### 3.8.1.2.2 THE VNL TOOLBAR

When we launch Virtual NanoLab (VNL), the first thing which appears is the **VNL Toolbar** window. The Toolbar provides access to all the individual tools that are used in VNL. These are summarized below in Table 3.1.

**Table 3.1 Summary of the Description of Virtual Nano Lab (VNL)**

| Tools | Icon | Description |
|---|---|---|
| Atomic Manipulator |  | Set up two-probe systems and make modifications to magnetic tunnel junctions. |
| Molecular Builder | 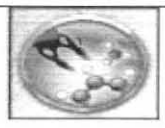 | Enables to build and construct molecules ready to be used in other VNL tools |

| | | |
|---|---|---|
| Bulk Builder |  | Enables to build and construct bulk systems ready to be studied and analyzed with other VNL tools |
| NanoLanguage Scripter |  | Create complete calculation set-ups and store these as NanoLanguage scripts |
| Method Editor | 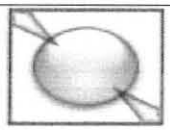 | Predefine DFT and NEGF parameters for re-use in the NanoLanguage Scripter when generating NanoLanguage scripts. |
| Script Editor |  | Manually edit and extend NanoLanguage scripts constructed by the different set of VNL tools |

### 3.9 Samples and Simulation Methods for Pristine and Aromatic Ring Attached AGNR with Width of 3, 6, 9 and 12.

We have prepared eight different two probe devices, four of which have no aromatic ring anchoring and four have aromatic $C_6$ ring attached with AGNRs. All the devices are connected to the left and right metallic lithium atomic-chain electrodes. The central region width is 11.11764 Å and the distance between the electrode atom (Li) and the C-atom of the central region is 2.00667 Å. The C-C bond lengths (1.42086 Å) in the $C_6$ ring is kept similar to that of the graphene as the ring is chalked out from the graphene only. Figure 3.1 show the two probe device for pristine and ring attached AGNRs having width 3 6, 9, and 12 respectively.

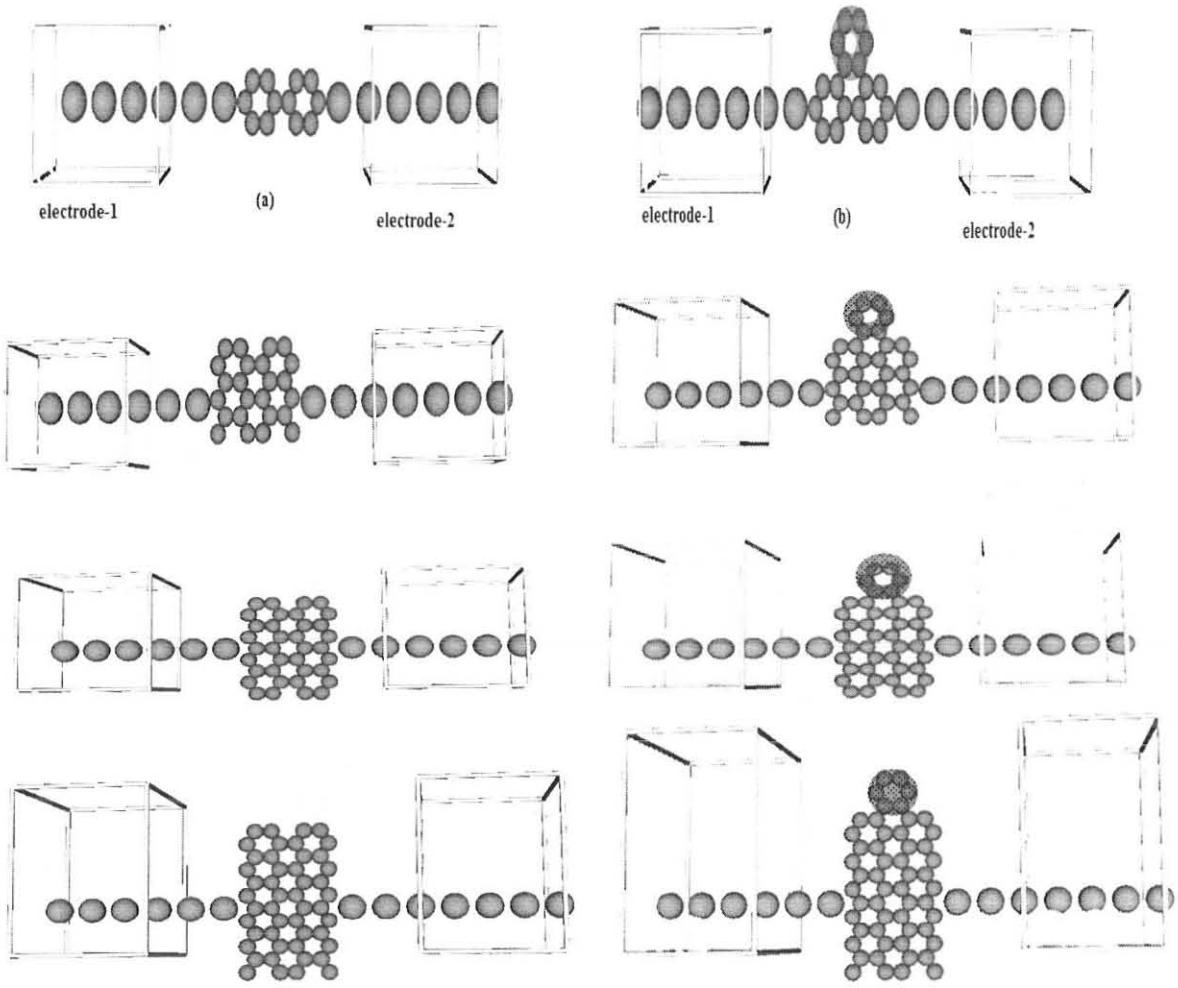


**Figure 3.1 Two probe devices for pristine and ring attached AGNRs having width 3 6, 9, and 12**

### 3.10 Script preparation

We have prepared scripts for the systems under study in separate files which are dragged and dropped into the Nano-Language scripter to set the desired parameters in order to simulate Density of states (DOS). The basis set with single zeta (Sz) type was set under method tab. Also for biased two probe system, electrode voltages were set across the left and right electrodes in between -2 V and 2 V with an interval of 0.5 V for current-Voltage measurements (I-V). A numerical calculation (.nc) file was created under the

self-consistent tab which stores results of each iteration step. And then an execution step for the Nano-Language script using a DOS command window was set to calculate the desired results. When the program execution terminated normally, a complete calculation file was obtained from the logout window. This file contains a huge data such as user defined conditions, initializing parameters and description about nano-structured system.

The self-consistent calculation calculates and compares the output values obtained after successive iterations. The results of DOS were stored in VNL files and are dragged and dropped in the result browser and nanoscope to be examined. In the Nano-Language script we set different parameters such as specify the check file name, analysis and methods in a two probe system. In the method we set parameters as shown in Table13.2

Table 3.2 **Basic Parameters used to simulate the different two probe device samples**

| Method used | Two probe method | |
|---|---|---|
| Basis set parameters | Type | Sz (Single zeita) |
| | Radial sampling dr | 0.001Bohr |
| | Energy shift | 0.01 Rydberg |
| | Delta R (inner) | 0.8 |
| | Vo | 40 Rydberg |
| | Charge | 0 |
| | Split Norm | 0.15 |
| | Element | All |
| Brilloun integration parameters | Number of k- points (A) | 1 |
| | Number of k- points (B) | 1 |
| | Number of k- points (C) | 500 |
| Exchange correlation | Exchange correlation Type | LDA.pz |
| Electron Density parameter | Mesh cutoff | 150.00 Rydberg |
| Two center integral parameters | Cutoff | 2500.0 Rydberg |
| | Number of points | 1024 |

| | | |
|---|---|---|
| Iteration Mixing parameters | Algorithm | Puly |
| | Diagonal mixing parameter | 0.1 |
| | Quantity | Hamiltonian |
| | History Steps | 6 |
| Iteration control parameters | Tolerance | 0.001 |
| | Criterion | Total energy |
| | Maximum steps | 400 |
| Energy contour Integral parameters | Circle points | 30 |
| | Integral lower bound | 3 Rydberg |
| | Fermi Function poles | 4 |
| Electrode Voltages | Voltage at Electrode 0 | 0.00V |
| | Voltage at Electrode 1 | 0.00V |
| Two probe Algorithm parameters | Electrode constraint | off |
| | Initial Density Type | Equivalent Bulk |

# CHAPTER-FOUR

## 4. Results and Discussions

In this chapter, we are concerned with presenting the simulation results from the atomistic calculations performed on the bare as well as the anchored armchair graphene nanoribbons (AGNRs). The discussion comprises the electronic band structures, the density of states (DOS), and current-voltage (I-V) characteristics based on two-probe systems. In the two-probe system, the central region comprises of pristine and aromatic ring attached AGNRs with widths of 3, 6, 9, and 12. In order to better understand the factors influencing the electronic and transport properties, fabrication of device with various widths is required. Various forms of chemical modification by $C_6$ ring anchoring to graphene nanoribbons can play a number of roles. Chemical modifications can also take place by substituting different atoms, adding functional groups or attaching different aromatic rings to the body of the graphene nano-ribbons; but here in this thesis, we are mainly focused on the $C_6$ anchoring on armchair edges of the ribbon. First we present our results for the reference samples which are devoid of any $C_6$ ring. Following this, we compare the results with $C_6$ ring anchored in the in-plane geometry with ribbons of various widths. We present and discuss the results of DOS performed on them.

### 4.1 Electronic Properties of Pristine AGNR

To understand the electronic structure of armchair graphene nanoribbons (AGNRs), we first calculated the band structure, Fermi energy and total energy of AGNRs with width 3, 6, 9, and 12. Figures 4.1 - 4.4 show the images, band structure , and bandgaps of pristine AGNRs with width of 3, 6, 9, and 12 having a repetition of 2 hexagonal rings and Tables 4.1 shows total energy, bandgaps, and types of transitions , and Table 4.2 shows bandgaps at different symmetry points of pristine AGNRs .

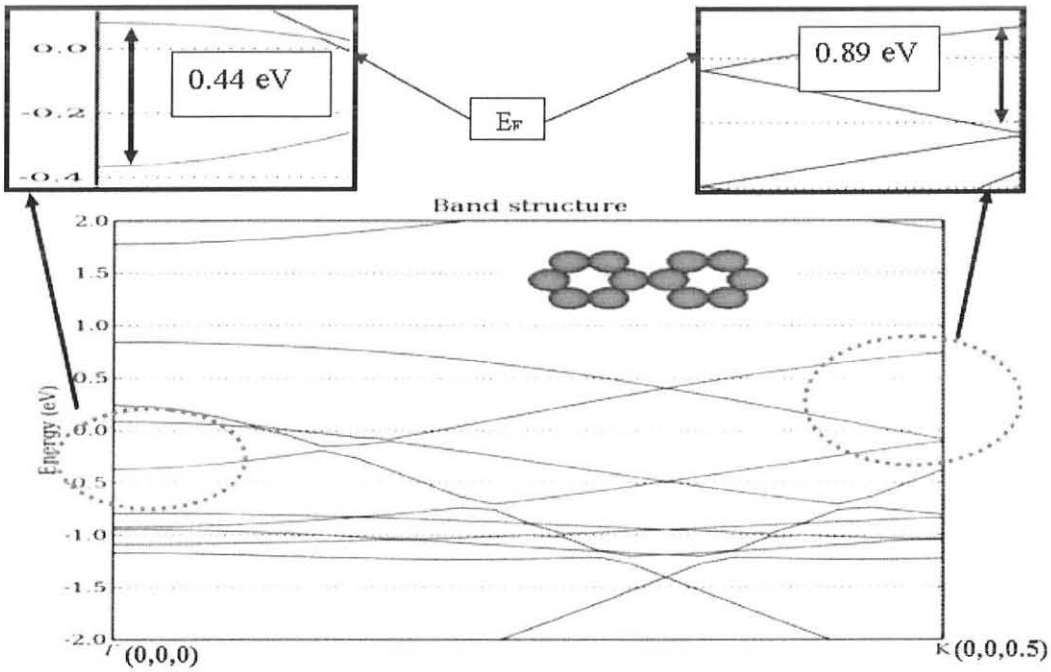


**Figure 4.1 Modeled sample of pristine 3 AGNR and its band structure**

In Figure 4 .1, the number 3 indicates the ribbon width. We can see from Figure 4.1 (LHS) that the LUMO (Lowest Unoccupied Molecular Orbital) is near to the Fermi level (0 eV). For the ribbon, which is essentially a one dimensional structure the Γ symmetry point basically represents momentum co-ordinates Γ (0,0,0) and the K symmetry point for the ribbon represents k (0, 0, 0.5). It is clear from the Figure 4.1 that LUMO-HOMO gap or the energy gap is smaller at the Γ-point. In addition, a more careful look at the band structure gives the lowest energy gap amongst the HOMO of K-point and LUMO of Γ-point transitions, which is found to be 0.23 eV. Furthermore, the LUMO at Γ-point is positioned near to the Fermi level, thus the material can exhibit n-type semi-conductivity.

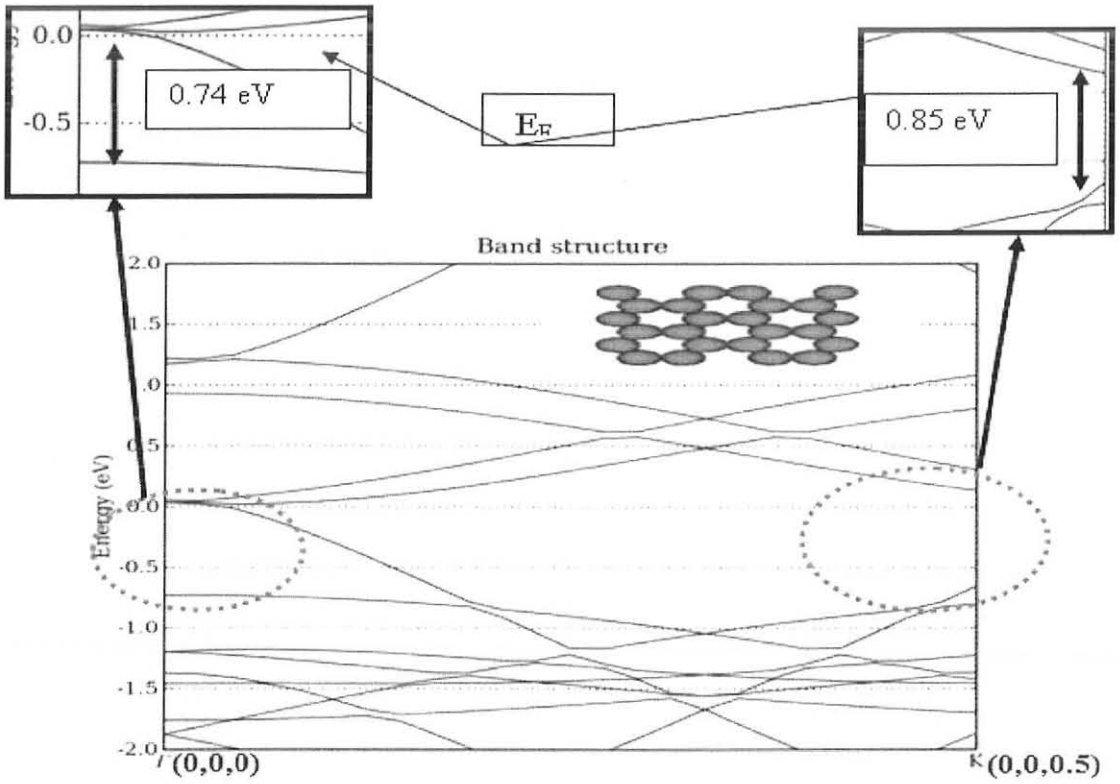


**Figure 4.2 Modeled sample of pristine 6 AGNR and its band structure.**

In Figure 4.2, 6 indicate the ribbon width. From the band structure of pristine 6 AGNR, we obtained the gap values of 0.74 eV and 0.85 eV, which shows its semiconducting nature. Also, the indirect transition is either absent in this sample or positioned at higher levels than that of direct ones. Thus, the 6 AGNR's band structure indicates that it is a semiconducting material with a non-zero direct band gap. The LUMO of 6 AGNR is also near the Fermi level than the HOMO (Highest Occupied Molecular Orbital). This again shows that the material is n-type semiconductor at the r-point.

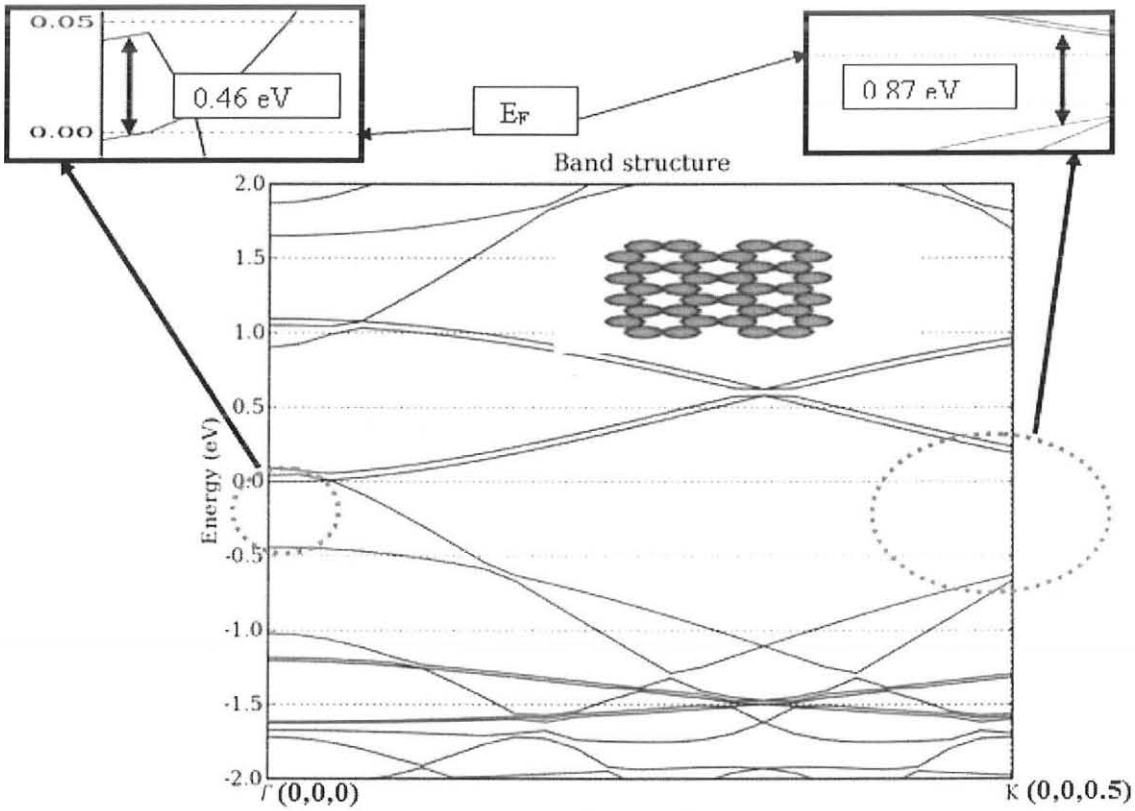


**Figure 4.3 Modeled sample of pristine 9 AGNR and its band structure.**

In Figure 4.3, the number 9 indicates the ribbon width. Interestingly, 9 AGNR's band-structure exhibits peculiar characteristics of armchair nanoribbons, which is the oscillation of the energy gap on increasing the width of the ribbon [34]. It should be noted that on increasing the width to 9 the energy gap further decreases to 0.46 eV and indicating towards the oscillatory dependence of the gap on the width for very small width ribbons (2-10 C-rows). The 9 AGNRs also found to be semi- conducting with a non-zero direct bandgap at the Γ→Γ energy transition.

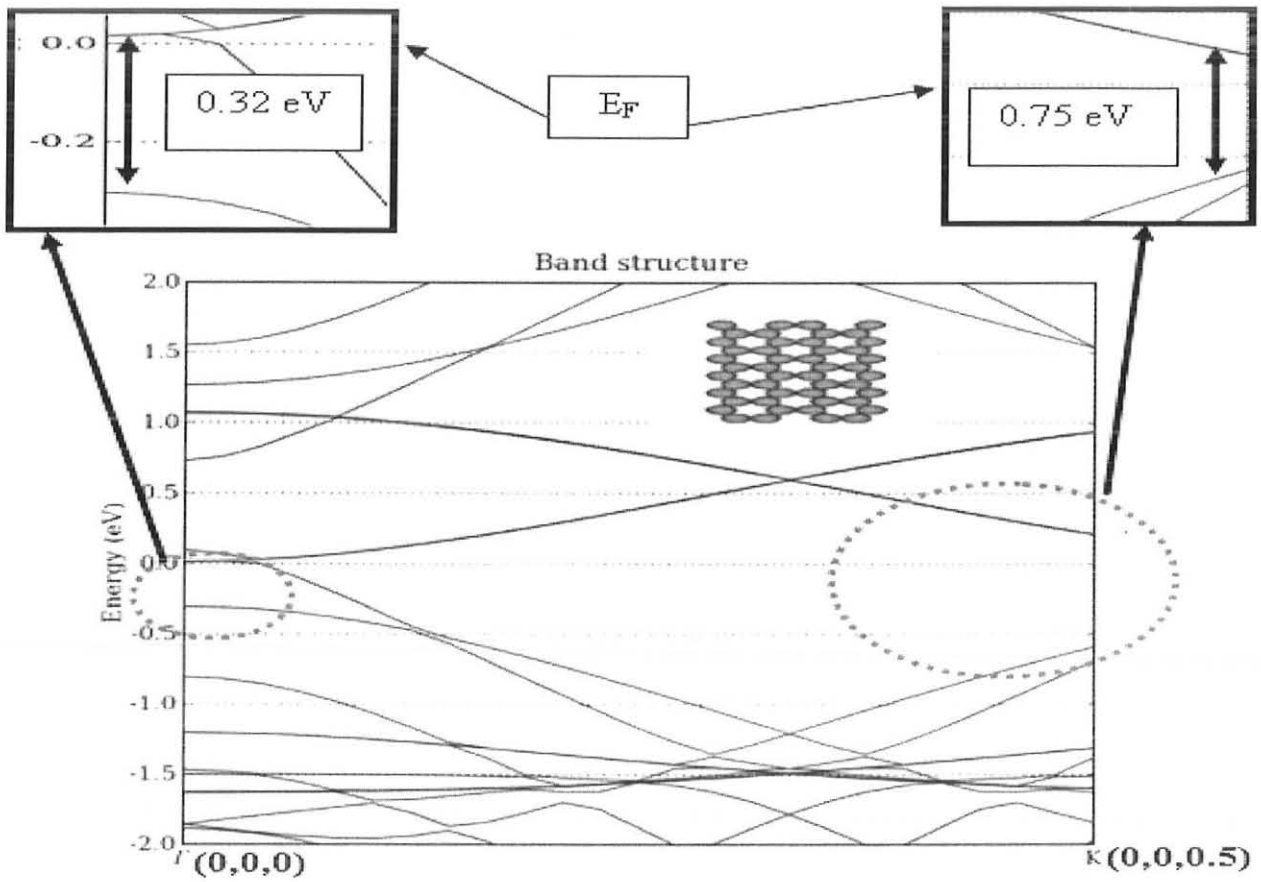


**Figure 4.4 Modeled sample of pristine 12 AGNR and its band structure**

For the ribbon of the width 12-C atom rows, the energy gap further reduces to 0.32 eV and the dominant transition remained to be Γ→Γ. Table 4.1 summarizes the various values of the energy transitions obtained at various symmetry points with the changing values of the ribbon widths.

**Table 4.1: Total energy, bandgaps and the type transition of pristine AGNRs**

| Width of AGNRs | Total energy (eV) | Bandgap (eV) | Type of transition |
|---|---|---|---|
| 3 | -1854.28 | 0.23 | Γ→K (Indirect) |
| 6 | -3733.37 | 0.76 | Γ→Γ(Direct) |
| 9 | -5612.56 | 0.46 | Γ→Γ (Direct) |
| 12 | -7491.76 | 0.32 | Γ→Γ (Direct) |

**Table 4.2: Bandgaps at different symmetry points in pristine AGNR**

| Samples | $E_{\Gamma-\Gamma}$ (eV) | $E_{\Gamma-K}$ (eV) | $E_{K-K}$ (eV) |
|---|---|---|---|
| 3AGNR | 0.44 | 0.23 | 0.89 |
| 6AGNR | 0.76 | 0.77 | 0.85 |
| 9AGNR | 0.46 | 0.68 | 0.87 |
| 12AGNR | 0.32 | 0.61 | 0.75 |

All the AGNRs usually show semiconductor characteristics with a non-zero direct band gap along the crystal symmetries present at Γ and K points [30]. This trend can be easily figured out from Tables 4.1 and 4.2. The bandgaps of AGNRs are found to vary with the change wi dth of the ribbons and they exhibit semiconducting characteristics at different crystal symmetry points. The total energies are also calculated for these AGNRs.Their total energies also increase with the increasing width showing an increase in stability of the ribbons. With the exception of the small width 3AGNR, all other width ribbons exhibit direct energy transitions. The indirect nature of the transition among very small width GNRs has also been recently reported elsewhere [35]. Another important trend that can be understood is that, in general, the bandgaps increases nonlinearly with the change in the width. The expected dependency of bandgap for the direct transition is expected to be an inverse of the square of the ribbon width that has also been previously reported [35]. Thus in agreement to the contemporary trends there is no monotonic bandgap narratives that are found among our pristine AGNR samples.

### 4.2 Electronic Properties of Aromatic Ring Attached AGNRs

It is expected that on attaching a ring to the graphene ribbon, a significant change in the electronic density of states and their energy dependency takes place due to the interplay of the charge transfer in between the ring and the ribbon. Figures 4.5 to 4.8 show the images of band structures and calculated bandgaps of ring attached AGNRs with ribbon width of 3, 6, 9, and 12 C-atoms. The results are further summarized in Table 4.3 shows the values of total energy, bandgaps, and types of transition ; and Table 4.4 depicts bandgaps at different symmetry points of ring attached AGNRs.

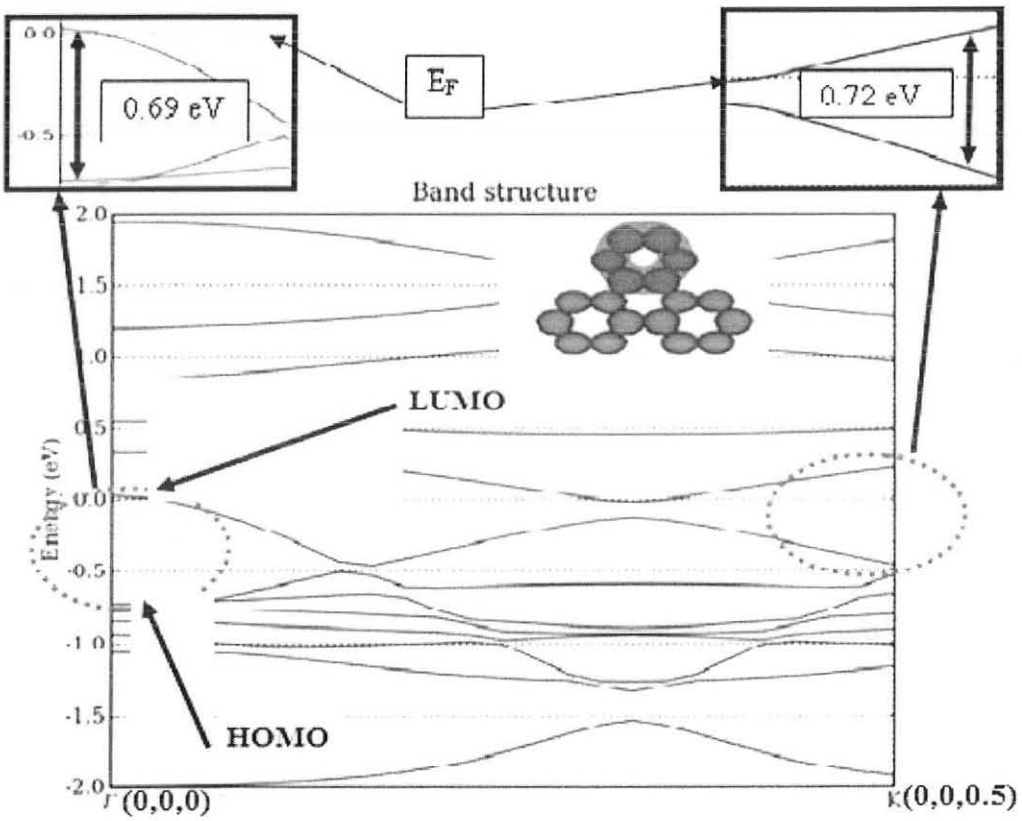


**Figure 4.5 Modeled sample of 3AGNR with ring and its band structure**

In Figure 4.5, the graphene ribbon width of 3 C-atom rows are used, which can also be seen from the inset schematic of Figure 4.5. With the attachment of the ring the direct energy gap at the Γ-point increases while at the K-point decreases, but the minimum gap

is for the indirect transition at Γ→ K with a value of 0.47 eV. Clearly, the LUMO is much near the Fermi level than the HOMO at zero value of electron momentum. Therefore, 3AGNR with ring attached is n-type semiconductor at the Γ-point.

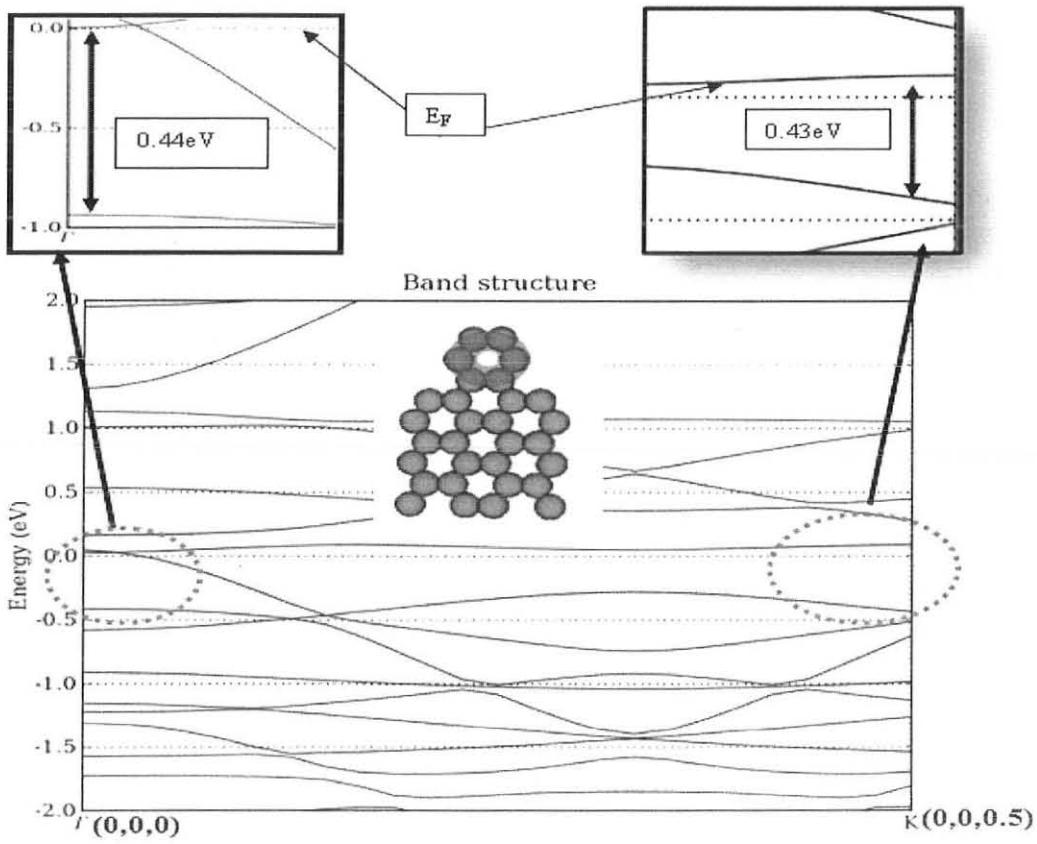


**Figure 4.6 Modeled sample of 6 AGNR with ring and its band structure**

In Figure 4.6, 6 - indicates the ribbon width. The energy gap minima are at gamma point with 0.44 eV, which is direct in nature. We can see from the band structure that the LUMO is closer to the Fermi level than the HOMO. This indicates 6 AGNR with ring attached is n-type semiconductor at the Γ-point.

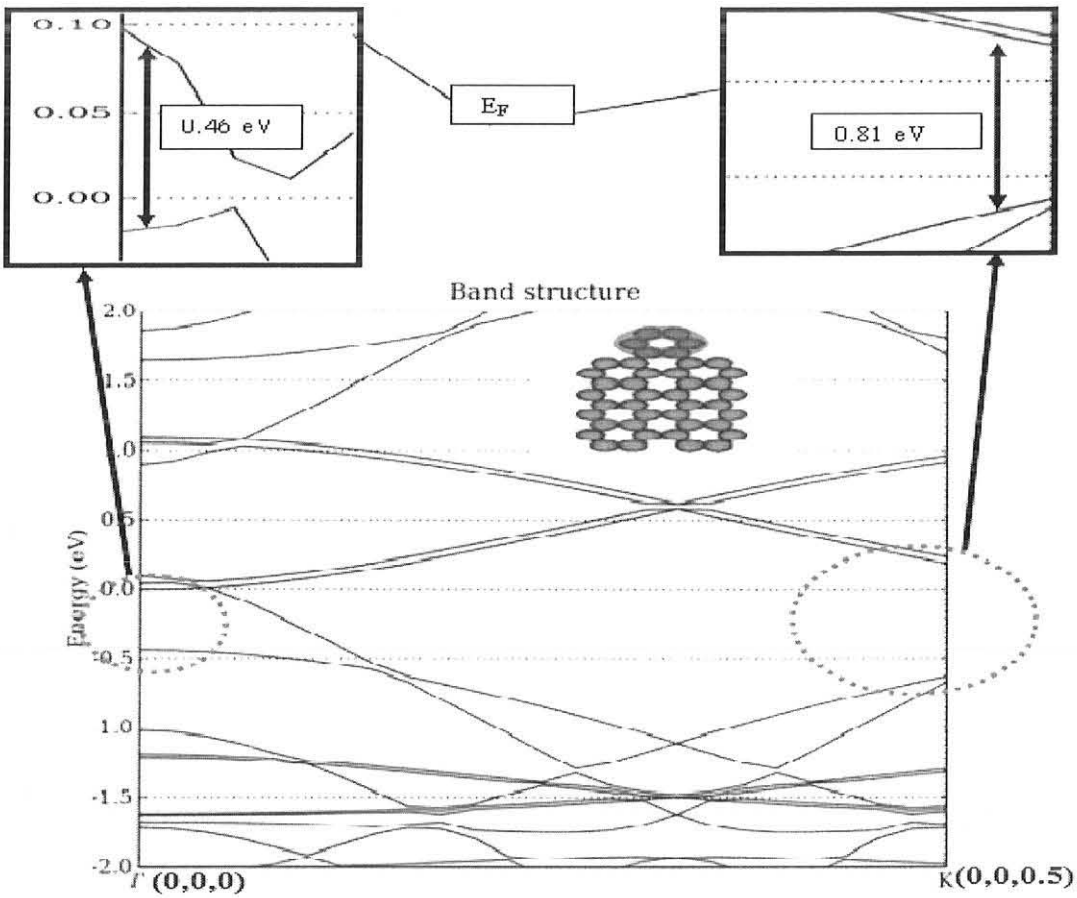


**Figure 4.7 Modeled sample of 9AGNR with ring and its band structure.**

From Figure 4.7, we observed that the LUMO is positioned near the Fermi level than the HOMO. Therefore, 9AGNR with ring attached is n-type semiconductor at the r-point. The energy gap minimum is at gamma point of 0.46 eV, which is direct in nature (the transition is from $\Gamma \rightarrow \Gamma$).

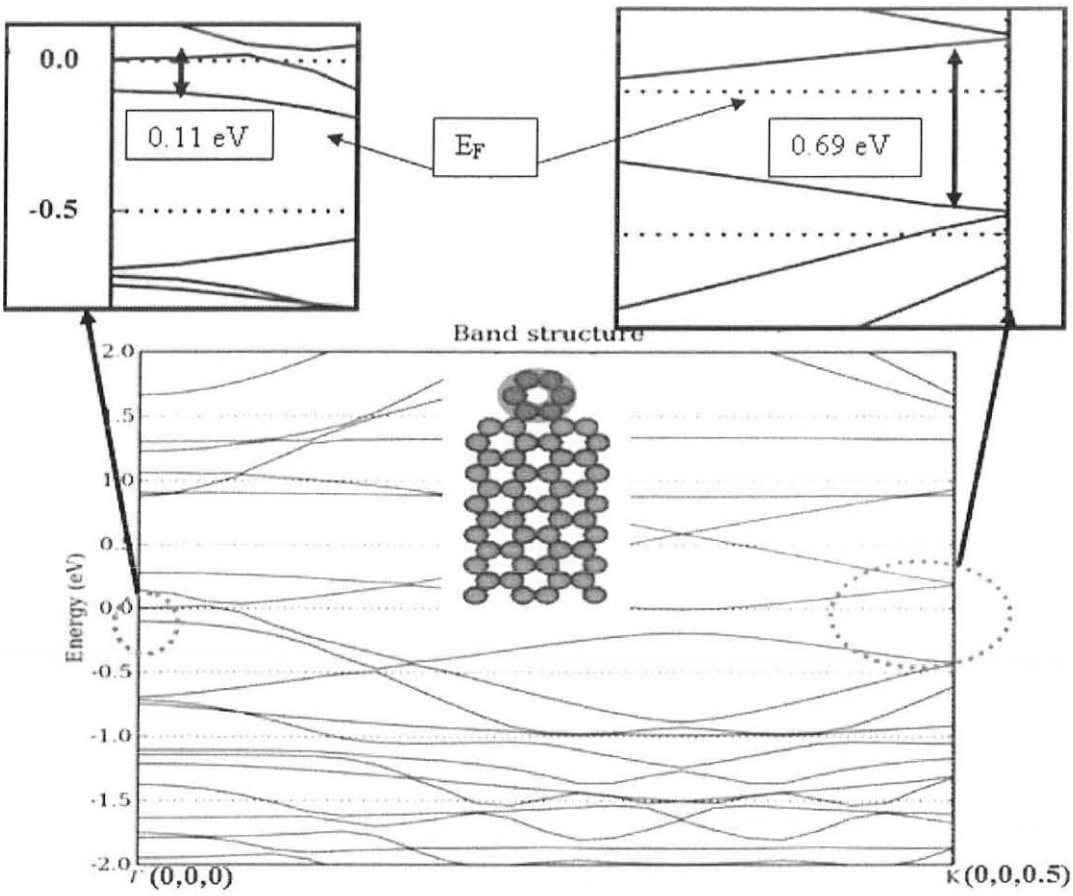


**Figure 4.8 Modeled sample of 12AGNR with ring and its band structure.**

From Figure 4.8 we can see that the LUMO is near the Fermi level than the HOMO. Therefore, 12 AGNR with ring attached is found to be n-type semiconductor at the Γ-point. The energy gap minimum is at gamma point with a smallest value of the ring attached GNRs of 0.11 eV, which is direct in nature ( the transition is fromΓ→Γ). The results of changes in the electronic properties of the ring attached to AGNRs of the various ribbon widths are summarized in Tables 4.3 and 4.4.

**Table 4.3: Total energy, bandgaps, and the type of energy transition of AGNRs with aromatic ring attached.**

| Width of AGNRs | Total energy (eV) | Bandgap (eV) | Type of energy transition |
|---|---|---|---|
| 3 | -2787.78 | 0.47 | Γ→K (Indirect) |
| 6 | -4356.62 | 0.44 | Γ→Γ (Direct) |
| 9 | -6545.22 | 0.46 | Γ→Γ (Direct) |
| 12 | -8115.03 | 0.11 | Γ→Γ (Direct) |

**Table 4.4: Bandgaps at different symmetry points in ring attached AGNRs**

| Sample | $E_{\Gamma-\Gamma}$ (eV) | $E_{\Gamma-K}$ (eV) | $E_{K-K}$ (eV) |
|---|---|---|---|
| 3AGNR | 0.69 | 0.47 | 0.72 |
| 6AGNR | 0.44 | 0.45 | 0.43 |
| 9AGNR | 0.46 | 0.65 | 0.81 |
| 12AGNR | 0.11 | 0.45 | 0.69 |

We have calculated the band structure for aromatic ring attached AGNRs of width 3, 6, 9 and 12. The band structures of aromatic ring attached AGNRs are found to vary with the width of the ribbons. As shown in Table 4.3, the highest bandgap calculated was 0.69 eV for 3 AGNR and the smallest band gap calculated was 0.11 eV for 12 AGNR. The calculated bandgaps showed that as the width of the ribbons get larger, the bandgaps oscillate but the effective value of bandgaps increase .as compared to their corresponding pristine AGNRs. In general, from the points we have discussed above, the bandgaps for the $N_a = 3p$ ribbons category where p = a positive integer (1, 2, 3, and 4) and $N_a$ is the number of dimer lines of the AGNRs , oscillates as the width of the ribbons increase. Hence, we predict that aromatic ring attachment on the ribbons increase the bandgap as compared to the bandgap for pristine AGNRs. Therefore, the effect of aromatic ring attachment on the ribbons with different width relatively increases the bandgap in comparison to those ribbons in which ring is not attached. This observation can be

attributed to the charge transfer among the ring and the parent nanostructure as a result of functionalization. There is also a difference in total energies between pristine AGNRs and aromatic ring attached AGNRs as indicated in Tables 4.1 and 4.3. The total energy gets larger for aromatic ring attached AGNRs than for pristine AGNRs, indicating their enhanced stability compared to their corresponding pristine AGNRs. We have also found that in both pristine and ring attached 3, 6, 9, and 12 AGNRs, the LUMO (the Low Unoccupied Molecular Orbital above the Fermi-level) is closer to the Fermi level than the HOMO (the High Occupied Molecular Orbital below the Ferm-level). Therefore, they are found to be n-type semiconductors (the charge carriers are mostly electrons) at the Γ-point. The results of the study of the charge transfer taking place among the functional group (ring) and the graphene nano-ribbon are summarized in Table 4.5

**Table 4.5 Electronic charge variations among Pristine and Ring attached AGNRs before and after functionalization**

| Samples | Pristine | | Ring attached | | | |
|---|---|---|---|---|---|---|
| | Initial charge of the ribbon | Final charge of the ribbon | Initial charge of the ring attached ribbon | Final charge of the ring attached ribbon | Initial charge of the ring | Final charge of the ring |
| 3AGNR | 48.0 | 47.9 | 48.0 | 47.99 | 24 | 24.01 |
| 6AGNR | 96.0 | 96.0 | 96.0 | 96.02 | 24 | 23.96 |
| 9AGNR | 144.0 | 144.0 | 144.0 | 143.90 | 24 | 24.09 |
| 12AGNR | 192.0 | 192.0 | 192.0 | 191.94 | 24 | 24.05 |
| Unit of charge= (e) = $1.6\times10^{-19}$C | | | | | | |

Table 4.5 shows that the small charge is transferred from the ribbon to the ring (~0.00636) and the energy gap value increases from previous indirect transition of 0.23

eV at Γ→K to the indirect transition with gap of 0.47 eV at Γ→K. Thus, the ring attachment manifests in the form of increased indirect energy gap without changing the nature of charge carrier transition. However, the ribbon with width of 6 again exhibits small charge acceptance from the ring and the decrease in the energy gap value to 0.44eV is observed for the Γ→Γ transition. It is to be noted that for the pristine 6 AGNR the minimum energy gap is for Γ→Γ transition at 0.76 eV. It should be recalled here that the small values of electronic charge transfer among the ring and small width ribbon (3 and 6) indicates weak functionalization. Interestingly, the strong functionalization is observed in the 9 AGNR and 12 AGNR samples with the corresponding higher charge transfer values of ~0.09e and ~0.05e. Besides, negligible change in the Γ→Γ energy transition is observed for the 9 AGNR and energy difference ΔE of 0.21 eV is found for bare and ring attached 12 AGNRs.

### 4.3 Two probe device measurements of Pristine and Aromatic Ring Attached AGNRs

It is a common observation that when nanostructures are connected with electrodes of a two probe device, their physical properties get changed to the charge transfer with electrodes. Now, I will present two probe sample devices result that I discussed before. . The AGNR two probe systems are simply constructed by placing AGNRs with proper width and repetition in between two electrodes, left (electrode-1) and right (electrode-2) as shown in Figure 3.1. In the simulation work for the two probe system, we have kept the number of left and right surface layers between the two electrodes fixed to be 4 to avoid charge reflections from the surface boundaries. This also resulted to have a width of 11.10 nm for the central region between the two electrodes. This simulation also finally gives the values of current for each applied bias voltage.

### 4.3.1 Comparison of I-V Characteristics of Pristine and Ring Attached AGNRs with Width of 3, 6, 9, and 12.

The most basic transport feature of nano-electronic devices is the one that is experimentally observable, which is the current voltage (I-V) characteristics. However, with the aid of current atomistic simulation techniques we can calculate the I-V characteristics by ab-initio formalism, as described earlier in Chapter 2. In the present I-V characteristics study, the base voltage across the central region through the 2-probes, which is a graphene ribbon is varied in between -2.0 V to 2.0 V with the interval of 0.5 V and a small current (in microamperes) is observed due to nano-dimensional nature of these devices. Figure 4.9 represents the I-V curve for 3 AGNR with ring attached and pristine. In a two probe device for 3AGNR with anchored aromatic ring, the I-V curve is almost linear current flow. It is to be noted that for pristine 3 AGNR, there is a large positive current for a bias voltage between 0 V and 0.5 V. For the bias voltage between 0. 5 V and 1.5 V, the current decreases; this is the manifestation of a phenomenon called negative differential resistance (NDR) [36]. However, the values of the current in the pristine 3AGNR are found to be higher than that of ring attached ribbon samples.

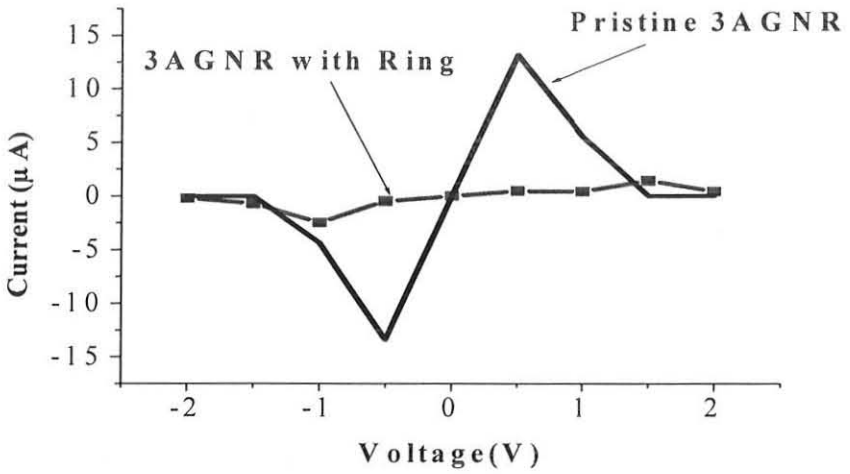


**Figure 4.9 I-V Curves for 3 AGNR with Ring and Pristine**

Thus, the ring attachment to the graphene has found to be the prominent effect on the ribbon's electrical conductivity. Also the ring attached 3-AGNR samples do not show clearly, w ell defined and displaced NDR peaks in comparison to that of the pristine ones, which indicates towards the changes in the electronic charge carrier density of the ribbon. These changes are mainly appeared due to the ring functionalization of the ribbon

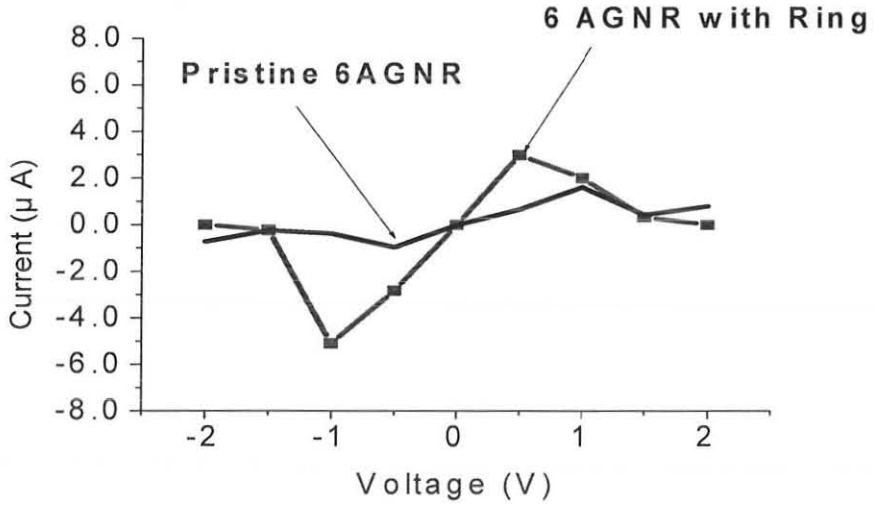


**Figure 4.10 I-V Curves of 6AGNR With Ring and pristine**

The I-V curve in Figure 4.10 shows a two probe device for 6 AGNR with ring attached and pristine. As it can be seen from the Figure, the current for pristine 6 AGNR is nearly linear indicating no current flow and the curve is oscillating but the current for 6 AGNR with ring increases for bias voltage between 0 V and 0.5 V and the current decreases as the bias voltage increases, a phenomenon called negative differential resistance. Therefore, 6 AGNR is somewhat good than its corresponding pristine one in its transport property.

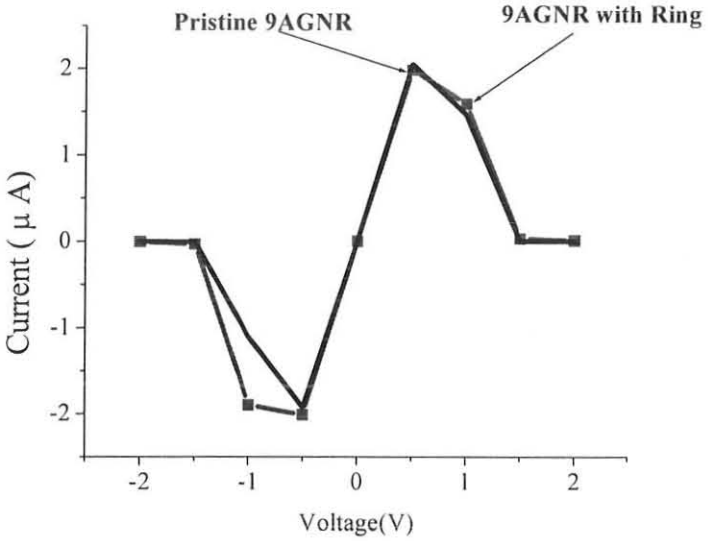


**Figure 4.11 I-V Curve of 9AGNR With Ring and Bare (pristine)**

Figure 4.11 represents the I-V curve in a two probe device for 9 AGNR with ring attached and pristine. From the I-V curve, we can see that in both cases the current increases for bias voltage between 0 V and 0.5 V. But for a bias voltage between 0.5 V and 1.5 V the current went down and become linear when the bias voltage >1.5 V. From the curve it is observed that pristine 9 AGNR; current is a little bit at the top than its corresponding ring attached one; eventhough the difference is negligible due to similarity in their bandgaps. This can be ascribed to the small change in the energy gap exchange with ring functionalization—both have similar values of ~0.46 eV.

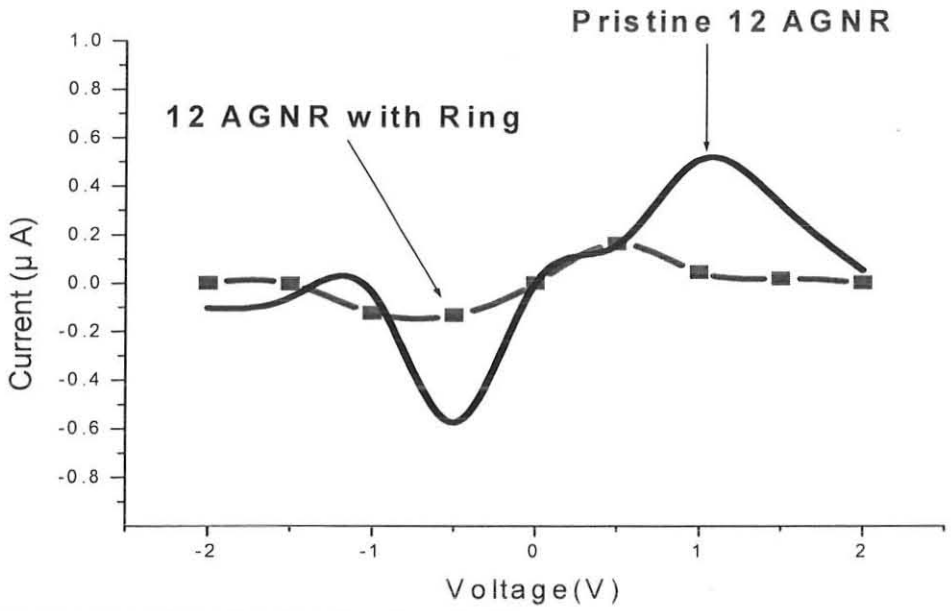


**Figure 4.12 I-V 12AGNR with Ring and Pristine**

The above I-V curve depicted in Figure 4.12 shows a two probe device for 12 AGNR with ring attached and pristine. In both pristine and ring attached 12 AGNR's, the I-V curve is oscillating (the curve moves or swings back and forth) but the current for 12 AGNR with ring decreases for bias voltage between -2 V and 0V and rises for bias voltage between 0 V and 0.5 V and then it decreases as the bias voltage increases and becomes linear. Therefore, pristine 12 AGNR passes more current than its corresponding ring attached one

## 4.4 Device Simulation of Density of States (DOS) Plots of AGNR Two-probe Systems

As stated earlier with the help of I-V results of the graphene ribbon devices that the changes in the values of the device resistance (current) or the displaced positions of the differential resistance present in the device is the changes in the carrier concentrations with the ring attachment. Hence, we are further presenting our direct calculation of the

charge carrier densities of states of pristine ribbon and the ring attached devices. The plot of DOS *vs* energy for 3 AGNR with ring attached and pristine is shown in Figure 4.13. As can be seen from the figure, pristine 3 AGNR has a longer peak at Fermi-level better than the ring attached one and its DOS is 2750 eV but the DOS with ring attached at the Fermi-level is 938 eV. This indicates there are more conduction states in pristine 3 AGNR than its corresponding ring attached 3 AGNR.

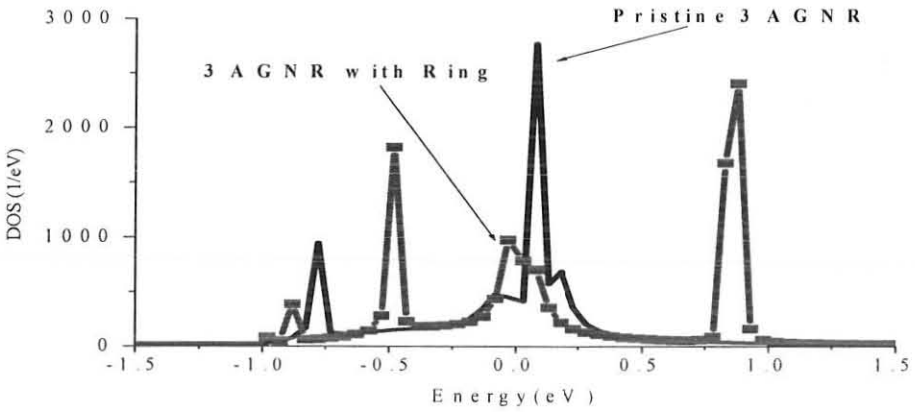


**Figure 4.13 DOS of 3 AGNR with Ring and Pristine**

The Figure 4.13 also depicts that pristine 3 AGNR has the largest conductivity as compared to the ring attached 3AGNR at the Fermi-level. In ring attached 3AGNR the conduction is contributed both by holes (p-type) and electrons (n-type) because we have nearly equal peaks to the left and right of the Fermi-level, whereas the charge carriers in pristine 3 AGNR are mostly the electrons (n-type). Less values of charge carrier concentrations in ring attached sample of ribbon of width 3, resonates in the form of the less current values of ringed sample as shown earlier in Figure 4.9.

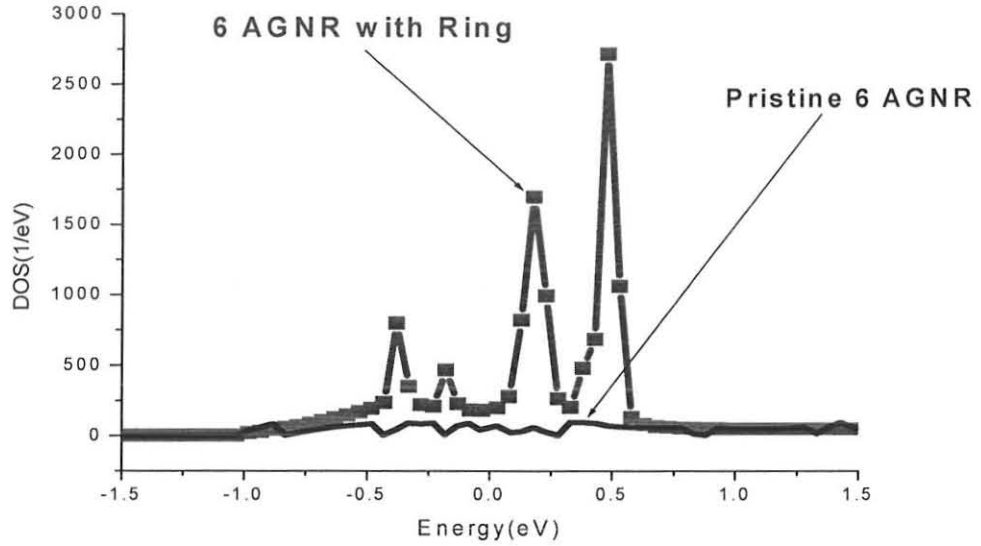


**Figure 4.14 DOS of 6AGNR with Ring and Pristine**

The DOS *vs* energy for 6 AGNR with ring attached and pristine is shown in Figure 4.14. If we look at Figure 4.14, the DOS for pristine 6 AGNR at Fermi level is 35.71 eV and that of ring attached at the Fermi level is 184.21 eV. For ring attached one for energy values between 0.0 eV and 0.6 eV, we have two peaks with DOS 1680.45eV and 2691.72eV to the right of the Fermi level. This shows that ring attached 6 AGNR has more DOS than its corresponding pristine 6 AGNR. Therefore, 6 AGNR with ring is better in conductivity than the pristine one. The charge carriers in both cases are the holes and electrons. Less values of charge carrier concentrations in pristine sample of ribbon of width 6, resonates in the form of the less current values of pristine as shown earlier in Figure 4.10.

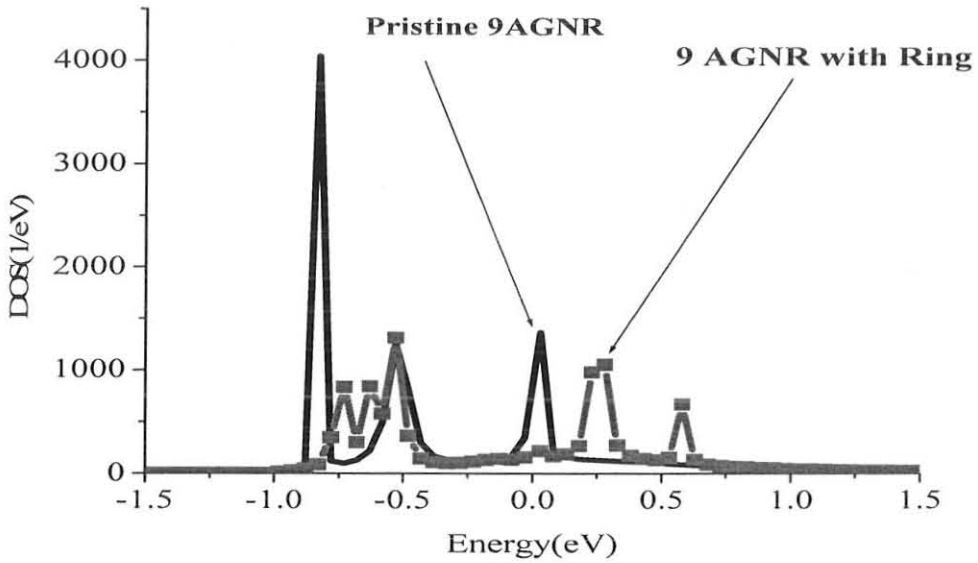


**Figure 4.15 DOS of 9 AGNR with Ring and Pristine**

The plot of DOS *vs* energy for 9 AGNR with ring attached and pristine is shown in Figure 4.15. There are DOS in both pristine and ring attached 9 AGNR at the Fermi-level; but DOS in the case of ring attached is insignificant. The DOS for 9AGNR with ring is found to be 219 eV and that of pristine 9 AGNR is found to be 1369 eV. This indicates that the DOS of pristine 9 AGNR is larger than that of 9 AGNR with ring and which in turn implies that there are more conducting states in pristine 9AGNR than that of 9 AGNR with ring. Nevertheless, these peaks are also characterized by narrow widths. To the left and right of the Fermi level there are peaks of ring attached 9 AGNR. This DOS indicates that the charge carriers in this case are both holes and electrons for this little conductivity (with DOS = 219 eV exactly at Fermi-level, 0.0 eV). But for pristine one the charge carriers are mainly the holes and the total charges among both pristine and functionalized samples are almost same. This shows the insignificant variations in their I-V characteristics as observed earlier.

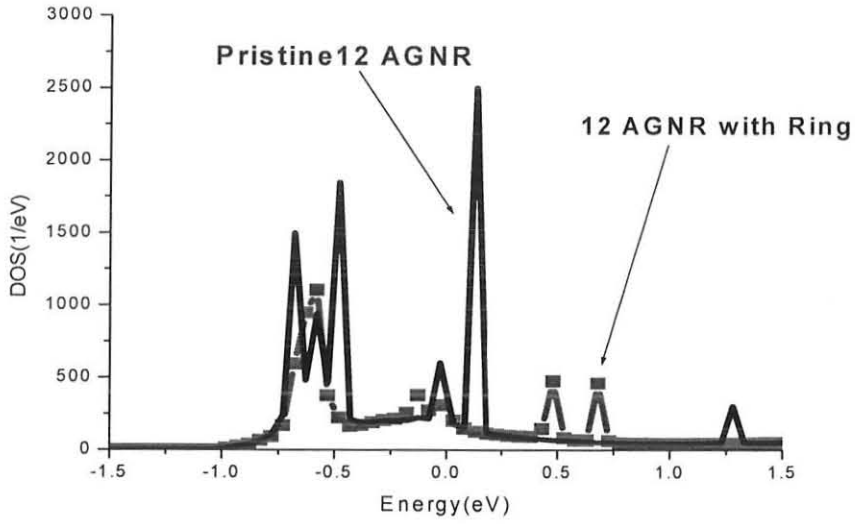


**Figure 4.16 DOS 12AGNR with Ring and Pristine**

As it can be seen from the Figure 4.16, there is DOS present for both pristine and ring attached 12 AGNR at the Fermi level. The DOS for 12 AGNR with ring is found to be 288.027 eV and that of pristine 12 AGNR is 563.907 eV. For pristine 12 AGNR, we have found more DOS to the left and right of the Fermi level than its corresponding ring attached one. Therefore, it is better in conductivity than its corresponding ring attached one. This observation is consistent with earlier reports as pure GNR devices [32, 33] which predicts the presence of resonance DOS modes at the zero points owing to the effects like fano resonance or strong coupling among various regions of the device [31]. The smaller values of charge carrier concentrations in the ringed sample of ribbon of width 12, resonates in the form of the less current values as shown in Figure 4.12.

**Table 4.6 Comparison of initial and final charges of the ribbon and the electrodes in pristine two probe system**

| Samples | Initial charge of the ribbon | Final charge of the ribbon | Initial charge of the left electrode | Final charge of the left electrode | Initial charge of the right electrode | Final charge of the right electrode |
|---|---|---|---|---|---|---|
| 3AGNR | 49.26 | 49.17 | 1.46 | 1.44 | 1.46 | 1.43 |
| 6AGNR | 97.16 | 97.18 | 1.46 | 1.45 | 1.46 | 1.40 |
| 9AGNR | 144.93 | 145.97 | 1.43 | 1.24 | 1.43 | 1.34 |
| 12AGNR | 193.72 | 193.61 | 1.32 | 1.33 | 1.31 | 1.19 |

*Unit of charge (e) = $1.6 \times 10^{-19}$ C

From Table 4.6, it is evident that there is a negligible charge transfer from the two probe electrodes to the central region that comprises of the first two types of AGNRs, 3 AGNR and 6 AGNR. It is to be remembered that there is less density of states for these ribbons from Figures 4.13 and 4.14, respectively. However in the case of 9 AGNR and 12 AGNR. we have found a significant value more than 1.0 eV and therefore, we get a strong coupling of ribbon to the electrodes of the device and there is a Fermi pinning induced large number of states (1369 eV) occurring exactly at the zero point of the DOS spectra as shown in Figure 4.15. Similarly, due to charge transfer and strong coupling between different regions of the device, we can see large DOS in Figure 4.16 of device 12 AGNR.

**Table 4.7 comparison of initial and final charges of the ribbon, electrodes, and the ring**

| Samples | Initial charge of the ribbon | Initial charge of the left electrode | Initial charge of the right electrode | Initial charge of the ring | Final charge of the ribbon | Final charge of the left electrode | Final charge of the right electrode | Final charge of the ring | Change in the charge of the ring |
|---|---|---|---|---|---|---|---|---|---|
| 3AGNR | 73.188 | 1.465 | 1.458 | 24 | 73.349 | 1.409 | 1.407 | 24.51 | +0.51 |
| 6AGNR | 113.399 | 1.368 | 1.353 | 24 | 113.508 | 1.288 | 1.287 | 23.983 | -0.02 |
| 9AGNR | 153.848 | 1.193 | 1.1929 | 24 | 170.281 | 1.405 | 1.391 | 24.06 | +0.06 |
| 12AGNR | 193.792 | 1.319 | 1.318 | 24 | 193.883 | 1.214 | 1.194 | 24.075 | +0.075 |

The negative sign in Table 4.7 (-0.02) indicates that the ring has given 0.02 e (charge) to the ribbon. The other positive values indicate that the ring has received charge from the ribbons. It is clear from the Table 4.7 that charge transfer is significant from the ring to the central region of 3 and 6 AGNRs but charge interaction with the electrodes is small. So in a small device region coupling, a significant variation with respect to the pristine ribbons DOS spectra is observed. We can observe new DOS peaks in 3 AGNR with ring attached on both of sides of the zero point as depicted in Figure 4.13. Due to the influence of ring, a completely new large DOS is observed at 0.8eV for the 3AGNR device. In short, we have observed increase in DOS for these two samples by the ring attachment, which is also evident from Figure 4.14, In 6 AGNR device new DOS peaks are observed especially at 0.5 eV, 0.25 eV, and -0.3 eV. However, DOS increase is not exactly at the Fermi level (zero point). So we can infer that ring attachment probably have no effect on the equilibrium conductivity of the device (compared to the pristine counterpart). Nevertheless the results are strikingly opposite in case of 9 and 12 AGNRs. It should be noted from DOS spectra of Figures 4.15 and 4.16, that zero density of states varies significantly from the values 1369 eV and 563.9 eV for pristine 9 and 12 AGNR to 219 eV and 288/eV for ring attached 9 and 12 AGNR, respectively. However, the overall DOS on either sides of zero point level remain fairly constant with or without ring

attachment from the table 4.7. It is clear that in case of 9 and 12 AGNRs the charge transfer is mainly from the electrodes to the ribbon. But in contrast to previous observation (from Table 4.6, the charge transfer between the electrodes and ribbons with width of 9 and 12 are high); here we do not have significant charge transfer from ring to the ribbon. Hence a strong device coupling is expected in 9 and 12 region which is also manifested in the form of higher equilibrium conductivity by ring attachment, as evident from their DOS spectra. But due to less interaction with ring there is no major change in DOS with ring attachment. Lastly, it should be noted that tabular values of the ring charge indicates that when the charge transfer values are positive the conductivity of the ringed samples increases to the higher value than that of their pristine counterparts. Furthermore, our I-V measurements are in complete agreement with this observation. We can also see this effect as in the case of 6 AGNR's I-V measurements (Figure 4.10), the current of pristine is lower than the ringed sample, the charge transfer in this sample is from the ring to the ribbon, which has possible increased the conductivity of the ribbon by inducing extra energy sub bands in the central region ribbon's 2 probe device.

## Conclusions

We have comparatively studied the electronic and transport properties of pristine and aromatic $C_6$ ring functionalized Armchair Graphene Nano Ribbons (AGNRs) with widths of 3, 6, 9, and 12 carbon-atom rows. A careful comparison of energy bandgaps and equilibrium conductivities has been performed. It has been found that on increasing the width of the pristine ribbon the bandgap do not decrease monotonically, but, it displays oscillatory decrease. From the band structure plots of the pristine and the carbon-6 ring attached armchair nano-ribbons it is found that the energy band decreases with the attachment of the ring and also the width dependency changes to monotonic in nature. Both the pristine and the ring attached ribbons are found to be direct bandgap materials at the Γ- crystal symmetry. However, the very small width ribbons (3 GNRs) are found to possess with indirect energy gaps at Γ→K transitions. All the armchair ribbon samples are always found semiconductors with a non-zero bandgap with n- type charge carrier conduction. Even, the covalent functionalization does not change the nature and type of conductivity in them. Nevertheless, the functionalization of the ribbon is found to be effectively tailoring the density of states spectra and the current-voltage (I-V) characteristics of the 2-probe nano-devices, which are fabricated by using the as-modeled pristine and ring attached nano-ribbons. All ring attached AGNRs have lower current transport properties than their corresponding pristine as ascribed to the observed strong functionalization $C_6$ ring with ribbons. A careful comparison of the I-V results has been made with the corresponding DOS spectra and all the results are found to be consistence with the DOS spectra of the devices. It is found that with the ring attachment DOS pattern changes and the net electrical conductivity of the ribbon decreases. From the facts we have observed , charge is transferred from the ribbon width of 3 ,9 , and 12 to the ring , which decreases the conductivity of the device. However, the ringed sample of 6 AGNRs shows exceptional results with higher values of conductivities in the ringed sample from their I-V plots. This is ascribed to the inverse values of charge transfer – from the ring to the ribbon. In general aromatic ring functionalization on the ribbons have two effects as shown by our simulation results; one of the effect is an increase in the

bandgaps of the ribbons and the other is a decrease in current transport properties of the ribbons due to the transfer of charges from the ribbons to the rings. Furthermore, to the best of our knowledge – for the first time – $C_6$ ring functionalization is discussed and dealt in the thesis.

**References:**


[1] Bianco A, Kostarelos K and Prato M, Chem Commun 5 (2005) 571

[2] Rajashree H, Manohar Y, Harshal G, Mohit V and Vilasrao K, Asian Journal of Pharmaceutical and Clinical Research 2 (2009) 0974

[3] Gorjizadeh N, Kawazoe Y and Farajian AA, Phys *Rev B.* 78 (2008) 155427

[4] Oxana VK and Boris IK, Open Inorganic Chem J 2 (2008) 39

[5] Castro Neto AH, Guinea F, Peres NMR , Novoselov K S and Geim AK, Rev Modern phys 81( 2009 ) 109

[6] Dubois SMM, Zanolli Z, Declerck X and Charlier JC, Eur Phys J B 72 (2009) 124

[7] URL: http://www.explainthatstuff.com/graphene.html, Retrieved on 10th March 2012

[8] Huang X, Qi XY, Boey F and Zhang H, Small 6 (2010) 513

[9] Virendra S, Daeha J, Lei Z, Soumen D, Saiful I. K and Sudipta Sl, Prog in Mater Science 56 (2011) 1178

[10] Wen QB, Yu SS, Zheng WT and Jiang Q, Molecular Simulation 34 (2008) 1085

[11] Barone V, Hod O and Scuseria GE, Nano Lett 6 (2006) 2748

[12] Son Y W,Cohen M L and Louie S G, phys Rev Lett 97 (2006) 216803

[13] Wang ZF, Li Q, Zheng H, Ren H and Su H ,Shi QW, Chin J Phys Rev B75 (2007) 113406

[14] Son YW, Cohen ML and Louie SG, Nature 444(2006) 347

[15] Gorjizadeh N and Kawazoe Y, J Nanomat 2010 (2010) 39

[16] Ruitao LV and Terrones M, Matter Lett 78(2012) 209

[17] Choi EY, Han TH, Hong J ,Kim JE, Lee S.H , Kim HW and Kim SO, J Mater Chem 20 (2010) 1907

[18] Rao CNR, Biswas K, Subrahmanyam KS and Govindaraj A, J Mater Chem 19 (2009) 2457

[19] Shao Y, Wang J, Hong WU ,Liu J, Aksay IA and Lin Y, Electroanalysis 22(2010) 1027

[20] Zhao JX, Wang H X , Gao BO , Wang X G, Cai QH and Wang XZ, J Mol

Model 18 (2012) 2861

[21] Chowdhury R, Scarpa F and Adhikari S, J Apl Phys, 112 (2012) 014905

[22] Matte HSSR, Subrahmanyam KS and Rao CNR, Nanomat Nanotech 1 ( 2011) 3

[23] Ejuh GW, Marie NJ and Singh AN, African Rev of Phys 6 (2011) 3

[24] Born M and Oppenheimer JR, Ann Physik 84 (1927) 457

[25] Capelle K, Brazilian J Phys 36 (2006) 1318

[26] Ao ZM and Jiang Q, Open Nano science Journal 3 (2009) 34

[27] Hai X, Jamil TK, and William AG, J. Phys. Chem. Lett. 2 (2011) 212

[28] ATOMISTIX TOOL KIT: Tutorial and Reference Guide, Version2.0 www.quantumwise.com./manuals/ATK-2.0.4-Tutorial-and-Refere, Retrieved on 15th February 2012.

[29] VirtualNanoLab: Tutorial, Version 2008.10, URL: www.quantumwise.com/

documents/manuals/vnl-2008.10-tutorial, Retrieved on 15th February 2012.

[30] Rozhkov AV, Nori F and Savelev S, Phys Rev B79 (2009) 125420

[31] Ezawa M, Phys Stat Sol 4 (2007) 489

[32] Mazzamuto F, Hung NV, Apertet Y, Caer C, Chassat C, Saint-Martin J and Dollfus P , Phys Rev B **83** (2011) 235426

[33] Wen C.X,Gang S Z, Chen B.J and Song K.H ,Chin Phys Lett 24(2007) 3225

[34] Tamar S, J Theoretical and Computational Chem 2 (2003) 439

[35] Ma F, Guo Z, Xu K and Chu PK, Sol. Stat. Commun. 152 (2012) 1089

[36] Kratochvilova I, Kocirik M, Zambova A, Mbindyo J, Mallouk TE and Mayer T S, J. Mater. Chem., 12 (2002) 2927